Volume 4, Issue 7 – July – December-2018

ECORFAN

Journal-Democratic Republic of Congo

ISSN-On line: 2414-4924

ECORFAN®

ECORFAN Journal-Democratic Republic of Congo, Volume 4, Issue 7, July-December 2018, is a journal edited semestral by ECORFAN. 6593 Kinshasa 31Rép. DémocratiqueduCongo.WEB:www.ecorfan.org/DemocraticRepublicofCongo/,journal@ecorfan.org. Editor in Chief: RAMOS-ESCAMILLA, María. Co-Editor: ILUNGA-MBUYAMBA, Elisée. MsC.ISSN On line: 2414-4924. Responsible for the latest update of this number ECORFAN Computer Unit. ESCAMILLA-BOUCHÁN, Imelda, LUNA-SOTO, Vladimir, 6593 Kinshasa 31Rép. Démocratique du Congo, last updated December 31, 2018.

ECORFAN- Democratic Republic of Congo

Definition of the Journal

Scientific Objectives

Support the international scientific community in its written production Science, Technology and Innovation in the Field of Physical and Mathematics Sciences and Earth Sciences, in Subdisciplines image and signal processing, digital-artificial control-system, Fuzzy-intelligence, mathematical-logic, computational-modeling, mathematical-computing, science.

ECORFAN-Mexico SC is a Scientific and Technological Company in contribution to the Human Resource training focused on the continuity in the critical analysis of International Research and is attached to CONACYT-RENIECYT number 1702902, its commitment is to disseminate research and contributions of the International Scientific Community, academic institutions, agencies and entities of the public and private sectors and contribute to the linking of researchers who carry out scientific activities, technological developments and training of specialized human resources with governments, companies and social organizations.

Encourage the interlocution of the International Scientific Community with other Study Centers in Mexico and abroad and promote a wide incorporation of academics, specialists and researchers to the publication in Science Structures of Autonomous Universities - State Public Universities - Federal IES - Polytechnic Universities - Technological Universities - Federal Technological Institutes - Normal Schools - Decentralized Technological Institutes - Intercultural Universities - S & T Councils - CONACYT Research Centers.

Scope, Coverage and Audience

ECORFAN -Democratic Republic of Congo is a Journal edited by ECORFAN-Mexico S.C in its Holding with repository in Bolivia, is a scientific publication arbitrated and indexed with semester periods. It supports a wide range of contents that are evaluated by academic peers by the Double-Blind method, around subjects related to the image and signal processing, digital-artificial control-system, Fuzzy-intelligence, mathematical-logic, computational-modeling, mathematical-computing, science with diverse approaches and perspectives , That contribute to the diffusion of the development of Science Technology and Innovation that allow the arguments related to the decision making and influence in the formulation of international policies in the Physical and Mathematics Sciences and Earth Sciences. The editorial horizon of ECORFAN-Mexico® extends beyond the academy and integrates other segments of research and analysis outside the scope, as long as they meet the requirements of rigorous argumentative and scientific, as well as addressing issues of general and current interest of the International Scientific Society.

Editorial Board

Arbitration Committee

ZACARIAS - FLORES, José Dionicio. PhD
Centro de Investigación y Estudios Avanzados

JIMENEZ - CONTRERAS, Edith Adriana. PhD
Instituto Politécnico Nacional

VILLASEÑOR - MORA, Carlos. PhD
Universidad Michoacana de San Nicolás de Hidalgo

REYES - RODRÍGUEZ, Aarón Víctor. PhD
Centro de Investigación y Estudios Avanzados

ANZUETO - SÁNCHEZ, Gilberto. PhD
Centro de Investigaciones en Óptica

GUZMÁN - CHÁVEZ, Ana Dinora. PhD
Universidad de Guanajuato

LÓPEZ - MOJICA, José Marcos. PhD
Centro de Investigación y Estudios Avanzados

IBARRA-MANZANO, Oscar Gerardo. PhD
Instituto Nacional de Astrofísica, Óptica y Electrónica

VAZQUEZ - PADILLA, Rita Xóchitl. PhD
Instituto Politécnico Nacional

CONDE - SOLANO, Luis Alexander. PhD
Centro de Investigación y Estudios Avanzados

VÁZQUEZ - LÓPEZ, José Antonio. PhD
Instituto Tecnológico de Celaya

KU - EUAN, Darly Alina. PhD
Centro de Investigación y Estudios Avanzados

JIMÉNEZ - GARCÍA, José Alfredo. PhD
Centro de Innovación Aplicada en Tecnologías Competitivas

CANO - LARA, Miroslava. PhD
Universidad de Guanajuato

CARBALLO - SÁNCHEZ, Álvaro Francisco. PhD
Universidad Autónoma de Puebla

PÉREZ - TORRES, Roxana. PhD
Universidad Tecnológica del Valle de Toluca

SANABRIA - MONTAÑA, Christian Humberto. PhD
Instituto Politécnico Nacional

OROZCO - GUILLÉN, Eber Enrique. PhD
Instituto Nacional de Astrofísica Óptica y Electrónica

TREJO - TREJO, Elia. PhD
Instituto Politécnico Nacional

MARTÍNEZ - BRAVO, Oscar Mario. PhD
Instituto Nacional de Astrofísica, Óptica y Electrónica

ZALDÍVAR - ROJAS, José David. PhD
Centro de Investigación y Estudios Avanzados

GARCÍA - RODRÍGUEZ, Martha Leticia. PhD
Centro de Investigaciones y de Estudios Avanzados

ARCINIEGA - NEVÁREZ, José Antonio. PhD
Universidad Nacional Autónoma de México

BARRAZA - BARRAZA, Diana. PhD
Instituto Tecnológico y de Estudios Superiores de Monterrey

BRICEÑO - SOLIS, Eduardo Carlos. PhD
Centro de Investigación y Estudios Avanzados

PANTOJA - RANGEL, Rafael. PhD
Universidad de Guadalajara

PARADA - RICO, Sandra Evely. PhD
Centro de Investigación y Estudios Avanzados

GARCÍA - GUERRERO, Enrique Efrén. PhD
Centro de Investigación Científica y de Educación Superior de Ensenada

Assignment of Rights

The sending of an Article to ECORFAN -Democratic Republic of Congo emanates the commitment of the author not to submit it simultaneously to the consideration of other series publications for it must complement the Originality Format for its Article.

The authors sign the Authorization Format for their Article to be disseminated by means that ECORFAN-Mexico, S.C. In its Holding Democratic Republic of Congo considers pertinent for disclosure and diffusion of its Article its Rights of Work.

Declaration of Authorship

Indicate the Name of Author and Coauthors at most in the participation of the Article and indicate in extensive the Institutional Affiliation indicating the Department.

Identify the Name of Author and Coauthors at most with the CVU Scholarship Number-PNPC or SNI-CONACYT- Indicating the Researcher Level and their Google Scholar Profile to verify their Citation Level and H index.

Identify the Name of Author and Coauthors at most in the Science and Technology Profiles widely accepted by the International Scientific Community ORC ID - Researcher ID Thomson - arXiv Author ID - PubMed Author ID - Open ID respectively.

Indicate the contact for correspondence to the Author (Mail and Telephone) and indicate the Researcher who contributes as the first Author of the Article.

Plagiarism Detection

All Articles will be tested by plagiarism software PLAGSCAN if a plagiarism level is detected Positive will not be sent to arbitration and will be rescinded of the reception of the Article notifying the Authors responsible, claiming that academic plagiarism is criminalized in the Penal Code.

Arbitration Process

All Articles will be evaluated by academic peers by the Double Blind method, the Arbitration Approval is a requirement for the Editorial Board to make a final decision that will be final in all cases. MARVID® is a derivative brand of ECORFAN® specialized in providing the expert evaluators all of them with Doctorate degree and distinction of International Researchers in the respective Councils of Science and Technology the counterpart of CONACYT for the chapters of America-Europe-Asia- Africa and Oceania. The identification of the authorship should only appear on a first removable page, in order to ensure that the Arbitration process is anonymous and covers the following stages: Identification of the Journal with its author occupation rate - Identification of Authors and Coauthors - Detection of plagiarism PLAGSCAN - Review of Formats of Authorization and Originality-Allocation to the Editorial Board-Allocation of the pair of Expert Arbitrators-Notification of Arbitration -Declaration of observations to the Author-Verification of Article Modified for Editing-Publication.

Instructions for Scientific, Technological and Innovation Publication

Knowledge Area

The works must be unpublished and refer to topics of image and signal processing, digital-artificial control-system, Fuzzy-intelligence, mathematical-logic, computational-modeling, mathematical-computing, science and other topics related to Physical and Mathematics Sciences and Earth Sciences.

Presentation of the Content

In the first chapter we present, *Interface based on computational geometry to characterize the spatial structure of point patterns for industry tools* by BAUTISTA-ELIVAR, Nazario, AVILES-COYOLI, Katia and MARTÍNEZ-SOLÍS, Luis with adscription in Tecnológico Nacional de México in the next section *Photocatalytic Degradation of 17α-Ethinylestradiol in Aqueous Solution* by NOGUERA-ORTIZ, Jonathan Eliezer, LUNA-SANCHEZ, Raúl Alejandro, SOLIS-MALDONADO, Carolina y ZERMEÑO-RESENDIZ, Brenda Berenice with adscription in the Universidad Veracruzana in the next section *Characterization of the catalytic activity and of luminescence in Ag/TiO_2 films* by TIRADO-GUERRA, Salvador and VALENZUELA-ZAPATA, Miguel, with adscription in the Escuela Superior de Física y Matemáticas del IPN in the next section an article *Optical and photocatalytic properties of TiO_2/ZnO composites* by TIRADO-GUERRA, Salvador and VALENZUELA-ZAPATA, Miguel, with adscription in the Escuela Superior de Física y Matemáticas del IPN.

Content

Article **ECORFAN Journal-Democratic Republic of Congo**
December 2018 Vol.4 No.7 1-7

Interface based on computational geometry to characterize the spatial structure of point patterns for industry tools

Interfaz basada en geometria computacional para caracterizar distribución de puntos espaciales en herramientas de uso industrial

BAUTISTA-ELIVAR, Nazario*†, AVILES-COYOLI, Katia and MARTÍNEZ-SOLÍS, Luis

Tecnológico Nacional de México/Instituto Tecnológico de Pachuca

ID 1st Author: *Nazario, Bautista-Eivar*/**ORC ID**: 0000-0002-9556-2748

ID 1st Coauthor: *Katia, Aviles-Coyoli*/**ORC ID**: 0000-0003-1619-4359 **CVU CONACYT ID:** 568518

ID 2nd Coauthor: *Luis, Martínez-Solís*/**ORC ID**: 0000-0002-0917-714X, **CVU CONACYT ID**: 929575

Received July 18, 2018; Accepted November 14, 2018

Abstract

Given a spatial point pattern, we propose a graphical interface is developed to analyze the spatial and angular characteristics based on Voronoi polygons and Delanuay triangles to extract information of the spatial point distribution of industrial tools, using Voronoi polygon and Delanuay triangulation (IVDI). This interface generate TXT files frequencies on Voronoi polygons, it generate graph which connects neighbors points in each Voronoi polygon selected by the user (Ulam tree modified) and it calculate the distances to each neighbor point and the internal angles. The interface obtain measures internal angles of Delanuay triangles, obtain measures neighbors nearest distance throughout the tesselation, obtain measures distance between selected points by the user, calculates the average of mean distances between points, evaluate polygonality and polygonality index, average angular differences, variation index of angle differences, mean-square deviation of angles, and circle radius circumscribing each Delanuay triangle.

Voronoi polygon, Delanuay trinangulation, Industries tools

Resumen

Dado un patrón de puntos espaciales, proponemos una interfaz gráfica para analizar las características espaciales y angulares basadas en polígonos de Voronoi y triángulos de Delanuay (IVDI) para extraer información de la distribución de puntos espaciales en herramientas de uso industrial, empleando polígonos de Voronoi y triangulación Delanuay. Esta interfaz genera archivos TXT de frecuencias de polígonos Voronoi, genera gráficos que conecta puntos vecinos en cada polígono Voronoi seleccionado por el usuario (árbol Ulam modificado) y calcula las distancias a cada punto vecino y grafico de ángulos internos. Mide los ángulos internos de los triángulos de Delanuay, mide la distancia más cercana a lo largo de la distribución de puntos, mide la distancia entre los puntos seleccionados por el usuario, calcula el promedio de las distancias medias, evalúa el índice de poligonalidad, media de diferencias angulares, índice de variación de las diferencias angulares, desviación cuadrática media de ángulos y radio del círculo que circunscribe cada triángulo de Delanuay.

Polígonos de Voronoi, Triangulación Delaunay, Diseño de herramienta industrial

Citation: BAUTISTA-ELIVAR, Nazario, AVILES-COYOLI, Katia and MARTÍNEZ-SOLÍ.S, Luis. Interface based on computational geometry to characterize the spatial structure of point patterns for industry tools. ECORFAN Journal-Democratic Republic of Congo 2018, 4-7: 1-7

* Correspondence to Author (email: nazariobel@itpachuca.edu.mx)
† Researcher contributing first author.

Introdution

Many applications in science, engineering, statistics, and mathematics require structures Voronoi diagrams, and Delaunay tessellations (J. Sudbø, 2000). These functions enable to geometrically analyze data sets in any dimension. Voronoi diagrams are a closest-point plotting technique related to Delaunay triangulation , which is useful by itself to create a triangular grid for scattered data points. Voronoi diagrams define a "natural mesh" for scattered data without explicit point connectivity (Luciano da Fontoura Costa, 2006, NoppadonKhiripe, 2012). Polygon mesh models are typically defined in terms of (a) geometry-the coordinate values of vertices of the meshes making up the model, (b) connectivity-the relationship among the vertices which defines the polygonal faces of the mesh (Iosif Pinelis, 2007). An interface with technology based in Voronoi polygons and Delaunay triangles is presented here to improve spaces setting industrial machines tools (IVDI). Given points grouped as a cloud, represent the tools, this interface is able to develop several graphics of proximity respect to the group of points already shown, this interface allows to obtain display and store from the optimization diagrams through the breaking down from the map in sections of tools.

Numerous researchers in various fields concern themselves with characterizing spatial distributions of objects. In these research fields, the point process theory undoubtedly helps dealing with these questions. Exploratory statistics of point patterns widely rely on Ripley's seminal work (Ripley 1976, 1977), namely the K function. A recent review of similar methods is given by Marcon and Puech (2014) who called them distance-based measures of spatial concentration. We will refer to them here as spatial structures since both dispersion and concentration points can be characterized.

The basic purpose of our interface (IVDI) is to test the observed point pattern against complete spatial randomness (CSR), i.e., a homogeneous Poisson process, to detect dependence between point locations (the null hypothesis supposes independent points) assuming homogeneity (i.e., the probability to find a point is the same everywhere).

Similar Ripley-like functions, available in the proposed R (R Core Team 2015) *dbmss* package (Marcon, Lang, Traissac, and Puech 2015), can be classified in three families:

– Topographic measures such as K take space as their reference (Fortin and Dale 2005).

– Relative measuressuchas M (Marcon and Puech 2010) compare the structure of a point type to that of another type (they can be considered as cases and controls).

– Absolute functions such as *Kd* (Duranton and Overman 2005) have no reference at all but their value can be compared to the appropriate null hypothesis to test it.

Methodology

Statistical background

We consider a map of points which often represents sections of tools. We want to apply to this point pattern a variety of exploratory statistics which are functions of distance between points and to test the null hypothesis of independence between point locations. These functions are either topographic, absolute or relative.

They can be interpreted as the ratio between the observed number of neighbors and the expected number of neighbors if points were located independently from each other. If reference and neighbor points are of the same type, the functions are univariate and allow to study concentration or dispersion.

Relative functions

Choosing reference and neighbor point types allows defining univariate or bivariate functions, counting neighbors up to or at a distance defines cumulative, using neighbors points of polygon Voronoi and Delanuay triangulation. Reference points are denoted x_i, neighbor points are x_j. For density functions, neighbors of x_i, are counted at a chosen distance *r*:

$$n(x_i, r) = \sum_{j,i\neq j} k\left(\left\|x_i - x_j\right\|, r\right)c(i,j) \qquad (1)$$

ISSN-On line: 2414-4924

$k(\|x_i - x_j\|, r)$, is a kernel estimator, necessary to evaluate the number of neighbors at distance r, $c(i,j)$ is an edge-effect correction (points located close to boundaries have less neighbors because of the lack of knowledge outside the observation window). In cumulative functions such as *M*, neighbors are counted up to *r*:

$$n(x_i, r) = \sum_{x_J \in N, i \neq} 1(\|x_i - x_j\| \leq r) w(x_j) \quad (2)$$

The number of neighbors is then averaged *n* is the number of reference points:

$$\bar{n}(r) = \frac{1}{n} \sum_{i=1}^{n} n(x_i, r) \quad (3)$$

Software description

Using $\bar{n}(r)$, we suggest development of an integrated platform based on computational geometry to study concentration or dispersion of points on tools, which in turn use both Voronoi tesselation and Delaunay triangulation, for the purpose to measure the distance, internal angles, radius of circumscribed circle, amid nearby points mean distances average, angular polygonality, polygonality index, mean-square deviation of angles, and variation index angle of differences. The platform holds two options, either being performed by a user or operating with an automatic formulations. This software allows to create Voronoi polygons and Delaunay triangles from a set of XY coordinates, or generated by selecting in an imported image. It locates XY coordinates, using an auxiliary window S, Fig**.** 1.

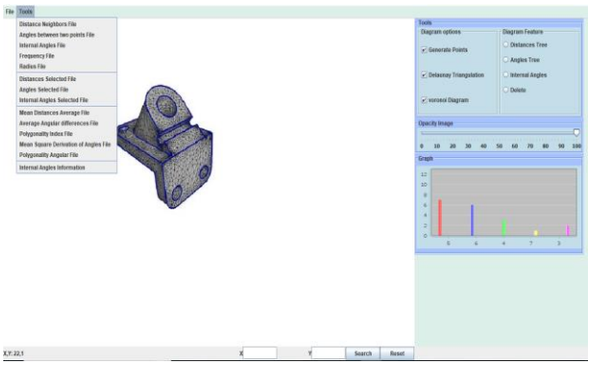

Figure 1 Platform based on computational geometry using Voronoi polygons and Delaunay triangles (IVDI).
Source: self made

Voronoi Frequency

This function displays graphics of frequency respecting to the number of sides in Voronoi mosaic with a data reading window, wider enough to avoid loss of data of polygons compared to other platforms (Image J).

Circumscribed Circle

These metrics/algorithms are able to find the magnitude of the circumradius, the coordinates of the center of the circumcircle, and the coordinates of the vertices formed in each Delaunay triangle. R is the radius of the circle circumscribing a Delaunay triangle, Fig. 2.

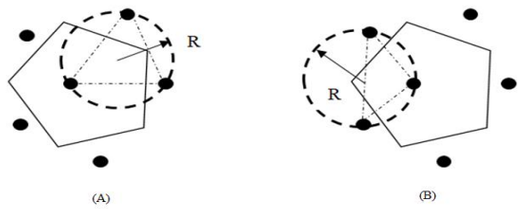

Figure 2 Circuncircle and circumradius for each Delanuay triangle in a Voronoi polygon
Source: self made

Distances Selected

These metrics/algorithms are able to get the distance (d_k) between each pair of points selected by the user. First select the icon distances, located in Diagram Feature screen, after that choose a point of the polygon, by the icon select points, then select again the icon select point for another interest point, finally activate the icon selected file distances from Tools menu to get the data file with its coordinates and the distance that separates them. You might select different pairs of points to find out their distances in a single file, activating the icon selected points, Fig. 3.

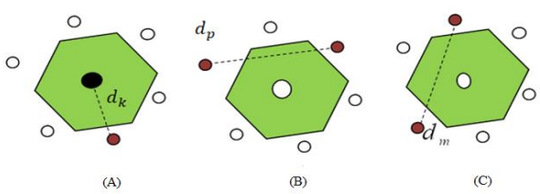

Figure 3 Distances to be chosen by the user in a Voronoi polygon
Source: self made

Angles Selected

These metrics/algorithms generate a file formed from each pair of points selected by the user. The angle υ is relative to the horizontal axis and it works as the rangefinder. First, activating angles tree icon (Fig.1), and then you can select different points for the same file using the select point button, to generate the Angles Selected file, Fig. 4.

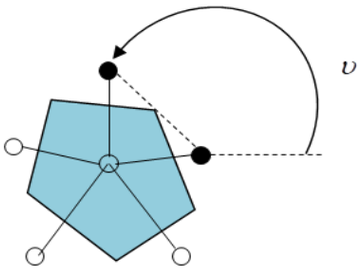

Figure 4 Selection of angles between neighbors to be chosen by the user in a Voronoi polygon
Source: self made

Internal Angles Selected

This metric algorithm generates a file for the angles γ_i of each Delaunay triangle selected by the user. First, activate radio button internal angles (Fig.5), then select points radio button to form the Delaunay triangle, selecting 3 points. The select order of each point defines the angle to be measured. First, if the black point is selected, then you can choose the white point, these two points form a line from which we start measuring the angle and ends at the line formed between the third point, striped circle, forming an angle which is measured from counterclockwise to clockwise, Fig. 5.

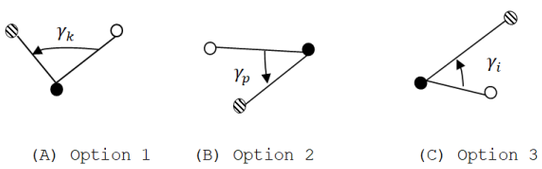

Figure 5 Select nearby points to get an angle between them in a Voronoi mosaic
Source: self made

Description of metrics/algorithm

Internal distance

The internal distance d_i in a particular Voronoi cell, is the distance measured from internal mathematical node (black dot, see Fig. 6) of the Voronoi polygon to each neighboring point (blue dot, see Fig.6) which forms the polygon. This is an Ulam tree modified to measure distances, Fig.6.

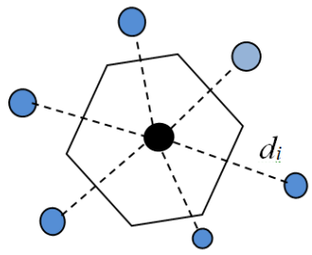

Figure 6 Distance graph (Ulam tree modified) between neighbors in a 6-tides Voronoi polygon
Source: self made

Angular graph

The numbers are the angles between the horizontal line which contains the internal mathematical node and the line which joins each neighboring point to the internal node, it is measured anticlockwise (Ulam tree modified to measure angles), Fig. 7.

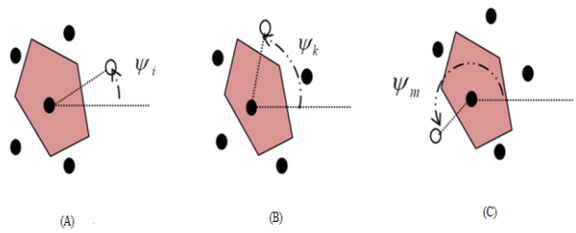

Figure 7 Measure angles between nearby points from a horizontal axis
Source: self made

Internal angles of Delaunay triangles

These are the internal angles of any triangle in the Delaunay triangulation ω_i ; the angles are measured in the positive direction (counterclockwise), Fig. 8.

ISSN-On line: 2414-4924

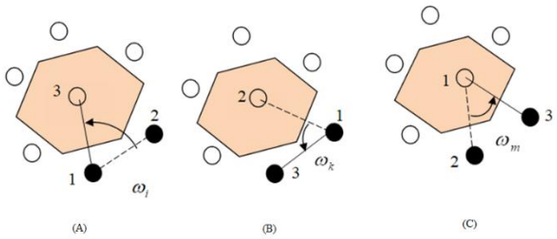

Figure 8 Measure angles between 3 neighbors that form a Voronoi polygon and choose one angle
Source: self made

The sequence to measure the angle ω_i is in the following order: if you select first point 1 (vertex 1) then select point 2 (vertex 2), these points will form a starting line where the angle measurement starts, the point 3 (vertex 3) is where the angle measured ends. The selection and sequence of generating points will indicate the final angle obtained.

Mean distances average

This metric/algorithm determine the mean of average distances from the inner point in every Voronoi cell to its *n* neighbors and it is calculated by $\sum_{i=1}^{n} \frac{d_i}{n^2}$, where d_i is the internal distance defined above. It also represents a way to measure the cell size and it could be interpreted as a coefficient of expansion or contraction, Fig. 9.

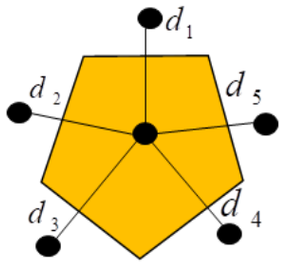

Figure 9 Modified Ulam tree graph for distances in each Voronoi cell
Source: self made

Polygonality Index

This metric/algorithm generates the measure of polygonality index, Eq. (4).

$$\Xi = \frac{1}{\sum_{i=1}^{n} |\chi_i - \beta| + 1}, \quad (4)$$

Where χ_i is the formed angle between consecutive neighbors for Delaunay triangle (irregular polygon, dotted arrow), β is the angle between consecutive vertex for a regular polygon (solid arrow), $\beta = 360^0/n$ and *n* is the number of neighbors from Voronoi cell, Fig. 10. Due to the way that χ_i is measured, its measurement is invariant under any rotation movement. The measurement is performed counterclockwise.

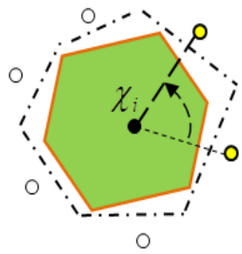

Figure 10 The solid line is a regular polygon, the irregular polygon is represented by the dotted line, and the neighbors are the black dots. The internal dot is a mathematical node
Source: self made

Mean-Square deviation of angles

This metrics/algorithms evaluate the mean-square deviation of angles, Eq. (5),

$$\varepsilon = \sqrt{\sum_{i=1}^{n} (\chi_i - \beta)^2}, \quad (5)$$

The root square of mean deviation from the angles χ_i, with respect to angle $\beta = 360^0/n$ where *n* is the number of neighbors of the Voronoi cell for each Voronoi polygon. The magnitudes χ_i , β , and *n* are defined above. Again, this measurement is invariant under any rotation movement.

Variation index angle of differences

This metric algorithm gets the Variation index angle of differences, Eq. (6),

$$\delta = 1 \Big/ \sqrt{\sum_{i=1}^{n} (\chi_i - \beta)^2} + 1, \quad (6)$$

Where χ_i , β and $\beta = 360^0/n$ are defined as above. If the value of δ is close to 1, then the Voronoi polygon is close to regularity, if δ is close to 0, then Voronoi polygon is irregular.

Results

Using the interface IVDI, we calculate $\bar{n}(r)$ by Eq. (3), for a metal gear, figure 11.

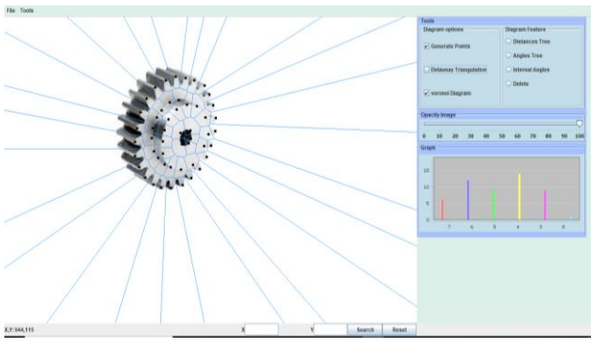

Figure 11 A metal gear
Source: self made

The *n* statistic is the sum of contribution of $\bar{n}(r)$ for all *r* values. $\bar{n}(r)$ are made independent by construction a metal gear. We want to evaluate the number of neighbors $\bar{n}(r)$ at distance *r*, for simulation, Ripley-like function and IVDI, figure 12.

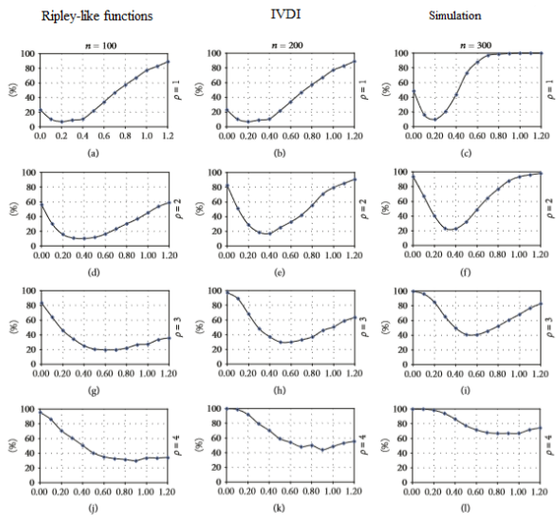

Figure 12 Several iterations to calculate % $\bar{n}(r)$, *n* is the number of simulated points for a metal gear, *ρ* aparameter of aggregation, X axis in cm
Source: self made

Taking into account distances above the maximun range of interaction between points limits the power of the test since a fraction of the $\bar{n}(r)$ values are purely stochastic. This is a normal behavior for a goodness-of-fit test. Ripley-like function test applied to a metal gear have a fit equal to 23.5%. In the same conditions, using IVDI, our test returns a fit value equal to 69.3%; it appears to close simulation of $\bar{n}(r)$ introduced in the analysis.

Conclusions

The platform is a tool based on computational geometry for getting structural manifestations and quantification of geometric distribution to characterize the spatial structure of point patterns for tools, based on Voronoi polygon and its dual Delanuay tesselation (IVDI). We built this package to provide an easy-to-use toolbox for users of spatial statistics mainly in tools employed on industries. Our results have goodness-fit that Ripley-like functions. The analysis is limited to testing a point pattern against an appropriate null hypothesis, including the simulation of many point processes as alternate null hypotheses and model fitting beyond exploratory statistics.

Future developments include the use of distance matrices as input of the distance-based functions to allow addressing of the simulation of many point processes. We will also develop subsampling techniques to be able to manage huge datasets (several million points) whose distances cannot all be calculated in a reasonable time.

References

Duranton G, Overman H (2005). "Testing for Localisation Using Micro-Geographic Data." Review of Economic Studies, 72(4), 1077–1106. doi:10.1111/0034-6527.00362.

Image J, https://imagej.nih.gov/ij/ , Open source. Iosif Pinelis, (2007). A characterization of the convexity of polygons in terms of cyclic the center angles, J. Geom, 87, Issue 1, 106-119.

Fortin MJ, Dale M (2005). Spatial Analysis. A Guide for Ecologists. Cambridge University Press, Cambridge.

ISSN-On line: 2414-4924

J. Sudbø, R. Marcelponil Reith (2000). New algorithms based on the Voronoi diagram applied in a pilot study on normal mucosa and carcinomas, Analytical Cellular Pathology, 21, pp. 71-86.

Luciano da Fontoura Costa, Fernando Rocha, Silene Maria Araujo Lima (2006); Characterizing polygonality in biological structures, Physical Review E 73, 011913-1,011913-10.

Marcon E, Puech F (2014). "A Typology of Distance-Based Measures of Spatial Concentration." Working Paper hal-00679993, HAL SHS. Version 2.

Marcon E, Lang G, Traissac S, Puech F (2015). dbmss: Distance-Based Measures of Spatial Structures. R package version 2.2.3, URL http://CRAN.R-project.org/package=dbmss.

Marcon E, Puech F (2010). "Measures of the Geographic Concentration of Industries: Improving Distance-Based Methods." Journal of Economic Geography, 10(5), 745–762. doi: 10.1093/jeg/lbp056.

NoppadonKhiripe, WongarnetKhantuwan, John R. Jungck, (2012) Ka-me: a Voronoi image analyzer, Bioinformatics, 28 (13): 1802-1804.

Ripley B (1976). "The Second-Order Analysis of Stationary Point Processes." Journal of Applied Probability, 13(2), 255–266. doi:10.2307/3212829.

Ripley B (1977). "Modelling Spatial Patterns." Journal of the Royal Statistical Society B, 39(2), 172–212.

ISSN-On line: 2414-4924

Article **ECORFAN Journal-Democratic Republic of Congo**
December 2018 Vol.4 No.7 8-15

Photocatalytic Degradation of 17α-Ethinylestradiol in Aqueous Solution

Degradación Fotocatalítica de Etinilestradiol en solución acuosa

NOGUERA-ORTIZ, Jonathan Eliezer†, LUNA-SANCHEZ, Raúl Alejandro*, SOLIS-MALDONADO, Carolina and ZERMEÑO-RESENDIZ, Brenda Berenice

Universidad Veracruzana, Facultad de Ciencias Biológicas y Agropecuarias. Carretera Tuxpan-Tampico km 7.5 Col. Universitaria, C.P. 92850, Tuxpan, Veracruz, México.

ID 1er Author: *Jonathan Eliezer, Noguera-Ortiz/* **ORC ID:** 0000-0002-1476-7363, **CVU CONACYT ID:** 621085

ID 1er Coauthor: *Raúl Alejandro, Luna-Sanchez/***ORC ID:** 0000-0003-2932-882X and **CVU CONACYT ID**: 265552

ID 2do Coauthor: *Carolina, Solis-Maldonado/* **ORC ID**: 0000-0002-9419-2001, and **CVU CONACYT ID**: 298580

ID 3er Coauthor**:** *Brenda Berenice, Zermeño-Resendiz/* **ORCID**: 0000-0003-0958-6450, and **CVU CONACYT ID:** 169262.

Received July 19, 2018; Accepted November 22, 2018

Abstract

In the present investigation work, the degradation of 17α-ethinylestradiol (EE2) in aqueous solution was studied. The main objective of this work is the degradation of EE2 through the process of heterogeneous photocatalysis using TiO_2 as a catalyst. The objective was the determination of the reaction parameters of the drug such as the photochemical effect, the adsorption rate of the catalyst and the initial concentration of the contaminant. The degradation was evaluated by the appropriate techniques of UV-vis and TOC spectroscopy. Like other works, the mineralization of this compound is reported, however, the % of EE2 mineralization can be determined in a solution that uses a photocatalytic process.

Degradation, Photocatalysis and 17α-etinilestradiol

Resumen

En el presente trabajo de investigación se estudió la degradación de 17α-etinilestradiol en solución acuosa. Como objetivo principal del presente trabajo es la degradación del EE2 mediante el proceso de fotocatálisis heterogénea utilizando TiO_2 como catalizador. Los objetivos particulares fueron la determinación de los parámetros de reacción del medicamento como lo son el efecto fotoquímico, índice de adsorción del catalizador y la concentración inicial del contaminante. Se evaluó la degradación mediante las técnicas adecuadas de espectroscopía UV-vis y TOC. Al igual que otros trabajos se reporta la mineralización de este compuesto, sin embargo, se logro determinar el % de mineralización del EE2 en solución acuosa utilizando un proceso fotocatalítico.

Degradación, Fotocatálisis y 17α-etinilestradiol

Citation: NOGUERA-ORTIZ, Jonathan Eliezer, LUNA-SANCHEZ, Raúl Alejandro, SOLIS-MALDONADO, Carolina y ZERMEÑO-RESENDIZ, Brenda Berenice. Photocatalytic Degradation of 17α-Ethinylestradiol in Aqueous Solution. ECORFAN Journal-Democratic Republic of Congo 2018, 4-7: 8-15

* Correspondence to Author (email: Raluna@uv.mx)
† Researcher contributing first author.

Introduction

A micro-contaminant is any compound present in soil and wastewater at concentrations expressed in µg/L and ng/L, which are persistent and resistant to conventional treatments and considered harmful to the environment. Among the micro-contaminants are pesticides, petroleum products and medicines [1-3].

Medicines have certain physicochemical characteristics and some of them are resistant to hydrolysis, to natural degradation and are considered highly disturbing for flora and fauna, also affecting abiotic factors by the alteration of pH, salinity, dissolved oxygen, etc. [4-6]. The inadequate final disposal of expired medicines causes the arrival to effluents, dissolved in wastewater, agricultural and veterinary use, being very difficult to eradicate [7-10].

Among the medicines that are commonly found in effluents, hormonal treatments are an alarming source, they are commonly used to alter the menstrual cycle and the impediment of conception, examples of such medications are EE2 (Figure 1) which is a synthetic estrogen compound that are used in contraceptive methods [11-18]. This compound is part of the so-called endocrine disruptors, which have the effect of simulating or altering the hormonal processes. These compounds cause a stress to the environment. Exposure to small amounts over prolonged periods can alter the development of fish tissues, are toxic to some species of algae, fish and invertebrates [19]. They can produce sexual inversion, reduction of the masculine sex and of the production of eggs, affecting the trophic chains and in some birds the thinning of the shell of eggs [20-24].

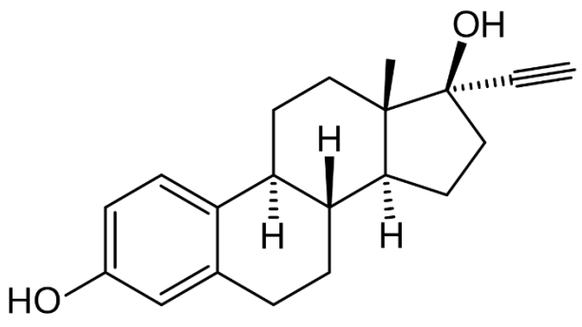

Figure 1 Chemical structure of 17α-ethinylestradiol. Chemical formula: $C_{20}H_{24}O_2$. And the molecular weight: 296.178 g/mol

Reports indicate the presence of concentrations between 1 and 5 ng/L of EE2 in different regions of the world, in surface waters and sediments have been detected in concentrations ranging between 1 and 100 ng/L [25-29]. Currently, it has been shown that EE2 has strong ecotoxic effects on the environment, in addition to interacting with other compounds, the byproducts generated can be harmful to wildlife, as well as the alteration of fish spawning cycles [29-31].

In recent years, advanced oxidation processes are an alternative to eliminate micro-contaminants. This set of techniques are physicochemical processes with the ability to produce structural changes in the chemistry of pollutants, because they involve the formation of powerful transient species such as hydroxyl radical, which allow the destruction of a large variety of organic compounds resistant to natural degradation. The hydroxyl radicals (OH) are highly oxidizing for organic matter and can be generated by photochemical processes either sunlight or radiant light, or by other forms of energy that do not involve radiant light [32-35].

Heterogeneous photocatalysis has been widely studied in the decontamination of wastewater and has proven its effectiveness for the degradation of medicines [33-36].

The photocatalyst TiO_2 presents physicochemical properties [37], which demonstrate a high efficiency for the elimination of a wide variety of contaminants including dyes, pesticides and medicaments [35,38,39,40-42].

Experimental

Chemical

The 17α-Ethinylestradiol (EE2) used for the photodegradation experiments is a white powder purchased from Sigma-Aldrich grade ReagentPlus (≥98%) with a solubility of 19 mg/L. For the photocatalytic experiments, commercial titanium dioxide TiO_2 Evonik-Degussa P25 with a composition of 80% anatase and 20% rutile was used. Also, distilled water and ethanol were used to prepare the EE2 solutions. For the analysis of total organic carbon, potassium biphthalate was used $C_8H_5O_4K$, sodium bicarbonate $NaHCO_3$ y sodium carbonate Na_2CO_3 TOC grade as reference standards.

ISSN-On line: 2414-4924

Photoreactor

The photodegradation experiments were carried out in a self-made system by the research group. Which consists of an annular cylinder of stainless steel with mirror finish, which supports 4 lamps of UV light brand Purikor of 16 watts. In the center of the system, a glass container is placed that functions as a batch reactor. The reactor is equipped with an oxygen supply and a magnetic stirrer to keep the reaction solution homogenized.

Photochemical Degradation Test

A photochemical degradation test was performed to monitor the effect of UV radiation on the contraceptive molecule under the established reaction conditions. The solution was maintained in constant magnetic stirring with a bubbling of oxygen saturated with a flow of 100 mL/minutes, at room temperature. Oxygen acted as an electron acceptor species throughout the experiment.

Adsorption Test

For this test, a load of 0.5 g of TiO_2 in a volume of 250 mL was used to evaluate the effect caused by a porous material such as TiO_2 in suspension in a solution of EE2 as a function of the change in the concentration of EE2 with respect to time. For this, the catalyst charge was added to the solution and kept under constant magmatic agitation for a period of 240 minutes in dark conditions. At every time care must be taken that the catalyst is not exposed to sources of light, for example, when weighing. It was also taken care that the solution was not exposed now of taking the samples or filtering them.

Photocatalytic Degradation Test

Solutions were tested with concentrations of EE2 at 5, 10 and 15 ppm, in each experiment the compound was previously diluted in 2 mL of ethanol using a 250 mL aqueous solution volume. A load of 0.5 g of TiO_2 exposed to UV irradiation is used in the reaction system for a period of 300 minutes, in which aliquots of 5 mL were taken, in addition to taking a pre-experiment sample without catalyst and in the times: 0, 15, 30, 45, 60, 90, 120, 180, 240 and 300 minutes, respectively.

The solution was kept homogenized by constant stirring, in addition saturated oxygen was supplied to the solution with a flow of 100 mL/minutes.

Analytical Methods

The progress monitoring of the reaction was performed by UV-vis spectroscopy using a JENWAY 7305 spectrophotometer; TOC analysis was also performed with a SHIMADZU TOC-5000A total organic carbon analyzer. Before analyzing each sample, it was centrifuged and filtered through Millipore GV membranes (0.22 μm pore diameter) to eliminate any traces of catalyst.

Results and Discussion

Photochemical Effect

The results of the photochemical effect indicate that the relative concentration of EE2 decreases 18% in 180 minutes of reaction, this does not represent a significant change, therefore, the contaminant shows resistance to photodegradation. The EE2 is a refractory compound which prevents the removal with light, therefore, it is necessary to use some advanced oxidation process [43-48].

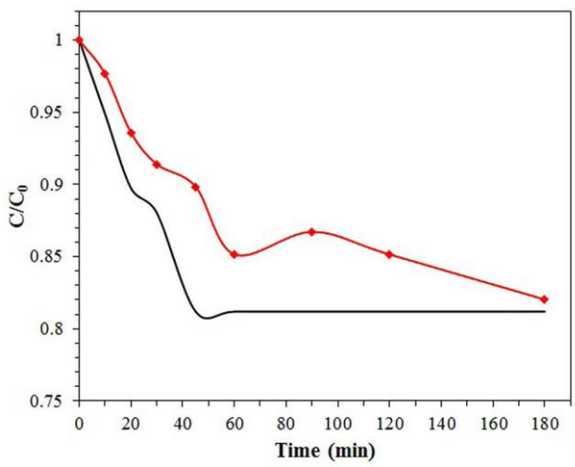

Graphic 1 Degradation profile of the photochemical effect as a function of the relative concentration at a concentration and index adsorption of the TiO_2 catalyst

Index Adsorption

The relative concentration profile of the adsorption experiment in dark conditions is presented in Graphic 1.

ISSN-On line: 2414-4924

The results of the adsorption test show a slight decrease in which it adsorbs approximately 19% during the first 45 minutes and subsequently reaches a state of equilibrium under these experimental conditions. This period of adsorption coincides with that reported by [49] in which it indicates 30 minutes and 10% adsorption with TiO_2 using lower concentrations of EE2 and amount of catalyst.

Photocatalytic Degradation with TiO_2

Relative concentration profiles by UV-vis spectroscopy indicate that the EE2 molecule degrades relatively easily in the first 300 minutes of reaction by the OH radicals generated in the photocatalytic process. Figure 3 shows that in the experiment of 5 ppm of EE2 there was a degradation of 99% in the 180 minutes. Meanwhile for the solution of 10 ppm of EE2 a degradation of 91.56% is shown in 240 minutes. The highest concentration of 15 ppm of EE2 reaches a degradation percentage of 76.40% at the end of the 300-minute experiment. These results could surpass that reported by [50] that reached a maximum percentage of 29% degradation for a concentration of 5 ppm of EE2. Other studies report higher percentages of photocatalytic degradation of EE2 using concentrations lower than those of this study [49].

The heterogeneous photocatalysis applied for the degradation of EE2 with TiO_2 turns out to be mostly efficient in comparison with other photocatalysts and the adsorption and electrochemical processes [51-54].

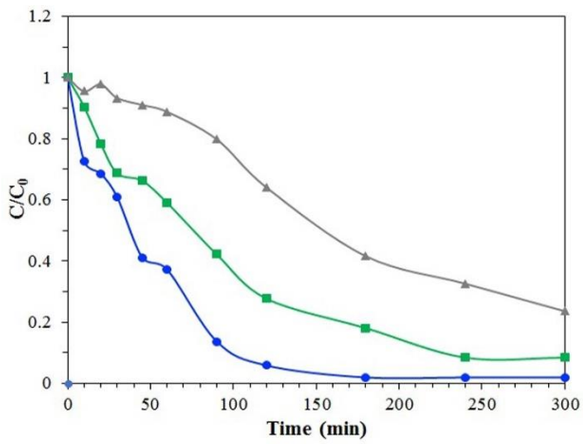

Graphic 2 Photocatalytic degradation of EE2 at different concentrations monitored by UV-vis spectroscopy (V=250 ml, TiO_2= 0.5g)

Total Organic Carbon (TOC)

The total organic carbon analysis was performed on the concentration experiments of 10 and 15 ppm of EE2 to monitor the degree of mineralization of the micro-contaminant. Graphic 3 shows a comparative graph showing that the mineralization profiles follow a similar behavior reaching 94% on average. In addition, the degree of mineralization of a known concentration of 15 ppm of EE2 is shown, which at the end of the reaction shows 95.52% total organic carbon values.

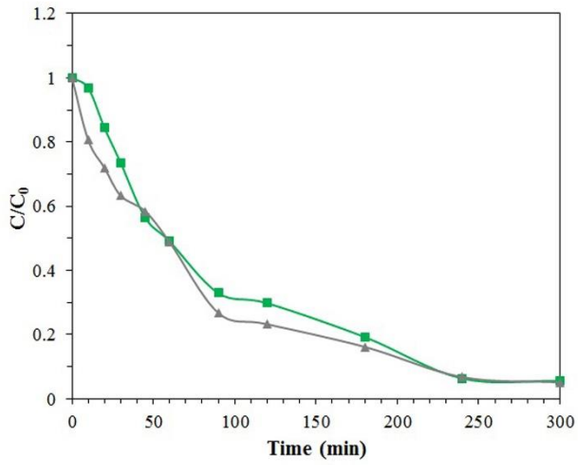

Graphic 3 Initial concentration efect on the photocatalytic mineralization of EE2 (V = 250 mL, TiO_2 = 0.5g, analyzed by TOC)

Chemical Kinetic

The results of the kinetic analysis of the reaction samples are shown in Graphic 4, indicating that the photocatalytic degradation of EE2 is adjusted to a first-order kinetic model, like other reports in the literature on this molecule [49, 55- 58]. Since the photocatalytic degradation reactions of organic compounds with aromatic character generates a series of organic products through a series-parallel mechanism [59]. The initial velocity of the photocatalytic degradation reaction of EE2 was determined, for which the velocity constant of a first-order reaction was evaluated using the initial concentration values of EE2 at times not greater than 180 minutes. Table 1 shows the kinetic parameters calculated as a function of the initial concentration of EE2.

ISSN-On line: 2414-4924

It is observed that the reaction rate constant decreases as the initial concentration of the contaminant increases and the rate of degradation of EE2 is inversely proportional to the initial concentration of the original reagent.

Initial concentration (ppm)	Initial concentration (mMol)	Apparent reaction constant kapar (min-1)	R^2	Reaction rate (-r) (mMol/min)
5	0.0168	0.3418	0.9045	0.0057
10	0.0337	0.1182	0.9841	0.0039
15	0.0500	0.0350	0.9532	0.0017

Table 1 Initial reaction rate as a function of the initial concentration in the photocatalityc degradation of EE2

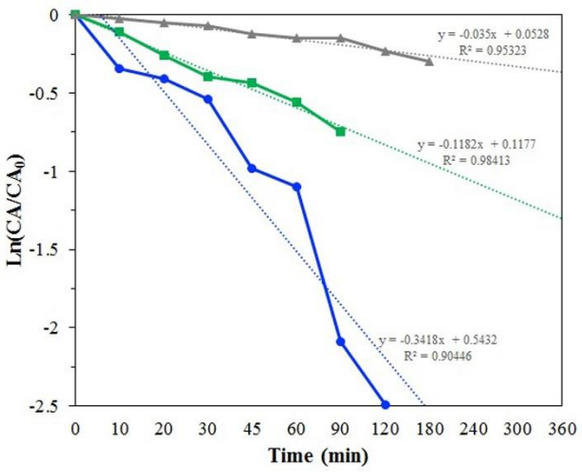

Graphic 4 Photocatalytic degradation kinetic model of EE2. C_0 = 5 ppm (blue line), C_0 = 10 ppm (green line), C_0 = 15 ppm (gray line). [V = 250 mL, TiO_2 = 0.5 g, analysis of samples by UV-vis spectroscopy]

Material Balance

By means of a material balance it is possible to determine the fraction of EE2 transformed to intermediate organic products in the photocatalytic degradation of the hormone. With the experimental results, the relative concentrations of EE2 are calculated with equations 1 and 2, respectively.

The fraction of EE2 mineralized to CO_2 is determined with equation 3, and the fraction of EE2 transformed to intermediate organic products is calculated with equation 4.

$$aC_m = \frac{C_m}{C_{m0}} \quad (1)$$

$$aTOC = \frac{TOC}{TOC_0} \quad (2)$$

$$fCO_2 = 1 - aTOC \quad (3)$$

$$fOIP = aCOT - aC_m \quad (4)$$

The intermediate organic products formation and consumption for the reactions of 5 ppm EE2 initial concentration is presented in Graphic 5. It is clearly seen that the fraction of intermediate organic products increases gradually as a function of time. After 120 minutes, the OH· radicals initially generated by the TiO_2 begin to attack the products of the reaction mixture, which decrease slightly and turn out to be persistent to the radical attack, because the profile remains almost constant until the end of the reaction. The products of the photocatalytic degradation of EE2 are widely reported by [49, 54]. In both articles, they propose that within the reaction mechanism the by-products generated conserve the original structure of EE2, therefore, it is necessary to increase the reaction time, to achieve total oxidation and environmentally harmless final products [60].

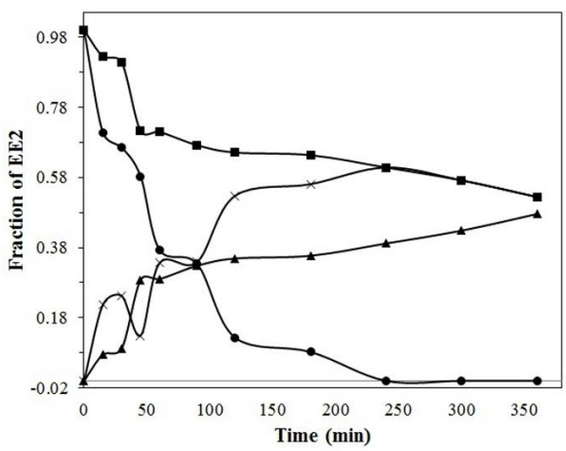

Graphic 5 Material balance for the photocatalytic degradation of EE2 in aqueous solution. (V = 250 mL, C_0 = 5 ppm, TiO2 = 0.5 g). ●= 17α-ethinylestradiol; ▲=Carbon Dioxide; ×= Organic Intermediates; ■= Total Organic Carbon

Conclusions

17α-ethinylestradiol (EE2) is not efficiently degraded by a photochemical process with UV light, the simple effect of radiation is not enough to eliminate this micropollutant in aqueous solution. The solution of EE2 with commercial TiO_2 Evonik-Degussa-P25 achieved its degree of saturation in 45 minutes, in this period the catalyst stops adsorbing the synthetic hormone and reaches its equilibrium point. The EE2 photocatalytic process in the presence of UV light, TiO_2 in a batch of photogravure was achieved with relative ease, a few minutes in reaction EE2 molecule is degraded by the action of the generated OH· radicals. The mixture of by-products generated at low levels are persistent to the oxidation and require long reaction times to convert them into CO_2 and H_2O. The photocatalytic degradation of EE2 is adjusted to a first-order kinetic equation.

Recommendations

The recommendations are that these and many others micropollutants of pharmaceutical origin continue analyzed due to their adverse impact on the environment sience it affects the biota and fauna as well as the entire trophic chain. Another recommendation for future works is to thoroughly analyze the intermediate products for a specific characterization, in the same way an analysis of ecotoxicity to see how harmful the metabolites of EE2 are, unlike the molecule initial.

Nomenclature

aC_m = Relative concentration of EE2

aTOC = Relative concentration of TOC

C_m = EE2 Concentration

Cm0 = Initial concentration of EE2

EE2 = 17α-Ethinylestradiol

fCO_2 = Fraction of mineralized EE2

fOIP = Fraction of organic intermediates products

K_{apar} = Kinetic reaction apparent rate constant
-r = Photocatalytic degradation reaction rate

TOC = Total organic carbon

TOC_0 = Initial total organic carbon

Acknowledgements

This project was partially funded by the Secretariat of Public Education through support for the promotion of the generation and innovative application of knowledge with official number: UV-PTC-859-511-6/17-8054.

Jonathan Eliezer Noguera Ortíz received the CONACYT Scholarship No. 621085 for postgrade studies. We thank the Photocatalysis Laboratory of the Faculty of Chemical Sciences of the Autonomous University of San Luis Potosí for the facilities of the use of TOC.

References

D. Barceló, M.J. López. Instituto de Investigaciones Químicas y Ambientales-CSIC. Barcelona, España. 2007.

M. J. Gil, A. M. Soto, J. I. Usma, O. D. Gutiérrez. Producción + Limpia 2012. 7(2), 52-73.

M. Stuart, D. Lapworth, E. Crane, A. Hart.Science of the Total Environment 2012. 416, pp. 1-21.

M. L. Richardson, J. M. Bowron. Journal Pharm Pharmacol. 1985, 37, 1-12.

K. J. Miller, J. Meek. Montana Bureau of Mines and Geology. Open- file report 532, 2006.

S. Pérez, D. Barceló. Analytical and Bioanalytical Chemistry, 2007, 387(4), pp. 1235-1246.

K. K. Barnes, D. W. Kolpin, E.T. Furlong, S. D. Zaugg, M. T. Meyer, L. B. Barber. Science of The Total Environment, 2008,404, 192-200.

H. C. Poynton, C. D. Vulpe. Journal of the American Water Resources Association, 2009, 45, 83-96.

A. J. Watkinson, E. J. Murby, D. W. Kolpin, S. D. Costanzo. Science of the Total Environment, 2009, 407(8), pp. 2711-2723.

L. I. Castro, M. I. Baños, M. A. López, B. L. Torres. Revista Mexicana de Ciencias Farmacéuticas, 2015, 46, 16-40.

ISSN-On line: 2414-4924

A. C. Johnson, A. Belfroid, A. Di Corcia. Te Science of the Total Environment, 2000, 256, 163-173.

M. Cargouët, D. Perdiz, A. Mouatassim-Souali, S. Tamisier-Karolak, Y. Levi. Science of the Total Environment, 2004, 324(1-3), pp. 55-66.

S. D. Kim, J. Cho, I. S. Kim, B. J. Vanderford, S. A. Snyder. Water Research, 2007,41, 1013-1021.

J. H. Writer, L. B. Barber, G. K. Brown, H. E. Taylor, R. L. Kiesling, M. L. Ferrey, N. D. Jahns, S. E. Bartell, H. L. Science on The Total Environment 2010. 409, 100-111.

E. Vulliet, C. Cren-Olivé. Environmental Pollution, 2011, 159, 2929-2934.

A. Jurado, E. Vázquez-Suñe, J. Carrera, M. López de Alda, E. Pujades, D. Barceló. Science of the Total Environment ,2012, 440, 82-94.

J. Y. Krein, C. Pailler, A. C. Guignard, L. Gutleb, B. Hoffmann, S. Meyer, P. Keβler, H. E. Berckmans, H. Witters. Environment and pollution, 2012, 1 (2), 86-96.

E. Aydin, I. Talinli. Chemosphere, 2013,90 (6), 2004-2012

S. B. Halling, N. S. Norson, P. F. Lanzky, F. Inherslev, L. H. C. Holten, S. E. Jørgensen. Chemosphere, 1998, 36, 357-393

R. M. Sharpe, J.S. Fisher, M. Millar, S. Jobling, J. P. Sumpter. Environmental Health Perspectives, 1995,103, 1136-1143.

J. P. Sumpter, S. Jobling. Environmental Health Perspectives, 1995, 173-178.

P. J. Patyna, R. A. Davi, T. F. Parkerton, R. P. Brown, K. R. Cooper. Science of The Total Environment, 1999, 233, 211-220.

K. E. Liney, J. A. Hagger, C. R. Tyler, M. H. Depledge, T.S. Galloway, S. Jobling. Environmental Health Perspectives, 2006. 114, 81-89.

C. R. Tyler, S. Jobling. Scientia et Technica, 2008, 50, 194-198.

D. W. Kolpin, E. T. Furlong, M. T. Meyer, S. D. Zaugg, L. Barber, H. T. Buxton. A National Reconnaissance, 2002. 36(6), 1202-1211.

R. Boxall, Q. Breton. Combinat Sci., 2003. 22, 212-221.

T. A. Ternes, M. Bonerz, N. Herrmann, B. Teiser, H.R. Andersen. Chemosphere, 2007. 66(5). 894-904.

E. Verledief, G. Cornelissen, B. Amy, H. Van der Gruggen, H. Van Dijk. Evironmental Pollution, 2007, 146(1). 281-289.

J. P. Besse, J. Garric. Environmental Pollution, 2009,157, 3485-3494.

P. F. Siegenthaler, P. Bain, F. Riva, K. Fent. Aqatic Toxicology 2017. 182 142-162.

X. Doménech, W. F. Jardim, M. I. Litter. Miguel A. Blesa (ed.). Ed. Gráfics 12 y 50, La Plata, Argentina, 2001.

G. Streck. Trends in Analytical Chemistry, 2009. 28(6) 635-652.

L. F. Garcés, E. A. Mejía, J. J. Santamaría. Revista Lasallista de Investigación, 2004. 1, 83-92.

L. F. Garcés, G.A. Peñalua. Revista Lasallista de Investigación, 2013, 2, 21-25.
B. J. Chamorro, C. P. Marín. Universidad de Cartagena, Cartagena, 2013.

R. Andreozzi, V. Carpio, A. Insola, R. Marotta. Catalysis Todayc, 1999, 53, 51-59.

T. N. Fujishima, D.A. Rao, T. D. Tryk. Journal of Photochemistry and Photobiology, 2000. C 1, 1-21.

M. Papamija, V. Sarria. Revista de Ingeniería, 2010, 31, 47-53.

R. A. Luna, B. B. Zermeño, E. Moctezuma, R. E. Contreras, E. Leyva, M. A. López. Revista Mexicana de Ingeniería Química, 2013, 12, 85-95.

J. A. Colina-Marquez, D. R. Castilla-Caballero. Chemical Engineering, 2013,15, 161-169.

ISSN-On line: 2414-4924

C. Aguilar, E. Moctezuma, C. Montalvo. International Journal of Environmental Research, 2011,5, 1071-1078, (ISSN 1735-6865).

H. Valencia, P.A. Reinosa, V. Arias. Scientia et Technica,2012. 50, 194-198.

D. Ren, B. Huang, D. Xiong, H. He, C. Meng, X. Pan. Journal of environmental sciences 2017. 54, 196-205.

E. J. Rosenfeldt, P. J. Chen, S. Kullman, K. G. Linden. Science of the Total Environmment 2007. 377, 105-113.

S. Canonica, L. Meunier, U. Von Gunten. Water Research, 2008,42, 121-128.

M. L. Janex-Habibi, A. Huyard, M. Esperanza, A. Bruchet. Water Research, 2009,43, 1565-1576.

N. Kim, H. Yamashita, T. Tanaka. Chemosphere, 2009, 77, 518-525.
X. L. Liu, Y. Kanjo, S. Mizutani. Science of the total environment, 2009, 407, 731-748.

Z. Frontistis, V. M. Daskalaki, E. Hapeshi, C. Drosou, D. Fatta-Kassinos, N. P. Xekoukoulotakis, D. Mantzavinos. Journal of Photochemistry and Photobioloy A: Chemistry, 2012, 240, 33-41.

D. Nasuhoglu, D. Berk, V. Yargeau. Chemical Engineering Journal, 2012, 185-186, 52-60.

Z. Zhang, Y. Feng, Y. Liu, Q. Sun, P. Gao, N. Ren. Journal of Hazardous Materials, 2012, 181, 1127-1133.

Z. Pan, E. A. Stemmler, H. J. Cho, W. Fan, L. A. LeBlanc, H. H. Patterson, A. Amirbahman. Journal of Hazardous Materials, 2012, 279, 17-25.

X. L. Liu, F. Wu, N.S. Deng. Environmental Pollution, 2003, 126, 393-398.

S. B. Fredj, J. Nobbs, C. Tizaoui, L. Monser. Chemical Engineering Journal, 2015, 262, 417-426.

H. M. Coleman, E. J. Routledge, J. P. Sumpter, B. R. Eggins, J. A. Byrne. Water Res. 2004. 38, 3233–3240.

G. L. Puma, V. Puddu, H. K. Tsang, A. Gora, B. Toepfer. Appl. Catal. B 2010. 99, 388–397.

W. L. Zhang, Y. Li, Q. Y. Wu, H. Y. Hu. Environ. Eng. Sci. 2012b. 29, 195–201.

Y. P. Zhang, J. L. Zhou. Chemosphere 2008. 73, 848–853.

H. De Lasa, B. Serrano, and M. Salaices. Springer. 2005, 978-0-387-2.

M. Carotenuto, G. Lofrano, A. Siciliano, F. Aliberti and M. Guida., Global Nest Journal., 2014, 20: 1-12.

ISSN-On line: 2414-4924

Article **ECORFAN Journal-Democratic Republic of Congo**
December 2018 Vol.4 No.7 16-26

Characterization of the catalytic activity and of luminescence in Ag/TiO_2 films

Caracterización de la actividad catalítica y de la luminiscencia en films de Ag / TiO2

TIRADO-GUERRA, Salvador*† & VALENZUELA-ZAPATA, Miguel

Escuela Superior de Física y Matemáticas del IPN, Edificio 9, U.P. "A.L.M." San Pedro Zacatenco, C.P. 07738, CDMEX, México. Laboratorio de Catálisis y Materiales, ESIQIE del IPN, Edificio 8, U.P. "A.L.M.", San Pedro Zacatenco, C.P. 07738, CDMEX, México.

ID 1st Author: *Salvador, Tirado-Guerra/***ORC ID:** 000-0001-9799-9963

ID 1st Coauthor: *Miguel, Valenzuela-Zapata/***ORC ID:** 0000-0002-8430-062X

Received July 10, 2018; Accepted November 27, 2018

Abstract

Ag/TiO_2 thin films are synthesized on soda-calcium glass substrates, using the sol-gel chemical route and repeated immersion. Series of TiO_2 films at a certain thickness, were modified superficially with several layers of Ag nanoparticles and thus obtaining the Ag/TiO_2 catalysts. The physical-chemical properties of the films are studied. The Ag/TiO_2 films were characterized by XRD and Raman spectroscopy, SEM morphology, chemical composition by EDS, the topography was recorded with AFM, its optical properties with UV-Vis and the ionic states of the surface components by XPS. The film thickness was 173.0 nm, a crystallite size of the order of 20 nm, a transmittance of 80%, a refractive index between 2.046-1.599, and Eg between 3.67-3.52 eV, depending on the surface modification with Ag. The catalytic activity was recorded evaluating the degradation of aqueous solution, depending on the concentration and time of irradiation with UV-Vis. The photoluminescence of the films was recorded when excited with photons of 325 nm. From the results of the study of Ag/TiO_2 films, they have the potential to be applied as catalysts in the treatment of contaminated water, and in radiation dosimetry.

Ag/TiO_2, Photocatalysis, Photoluminescence.

Resumen

Se sintetizan películas delgadas Ag/TiO_2 sobre sustratos de vidrio sodo-cálcico, usando la ruta química sol-gel e inmersión repetida. Series de películas TiO_2 a determinado espesor, se modifican superficialmente con varias capas de nanopartículas de Ag y se obtienen así los catalizadores Ag/TiO_2. Se estudian las propiedades físico-químicas de las películas. Las películas Ag/TiO_2 se caracterizaron por DRX y espectroscopia Raman, morfología por MEB, composición química por EDS, se registró la topografía con MFA, sus propiedades ópticas con UV-Vis y los estados iónicos de los componentes superficiales por XPS. El espesor de película resultó de 173.0 nm, un tamaño de cristalito del orden de 20 nm, una transmitancia del 80%, un índice de refracción entre 2.046-1.599 y el Eg entre 3.67-3.52 eV, dependiendo de la modificación superficial con Ag. Se registró la actividad catalítica evaluando la degradación de solución acuosa, en función de la concentración y el tiempo de irradiación con UV-Vis. Se registró la fotoluminiscencia de las películas al ser excitadas con fotones de 325 nm. De los resultados del estudio de las películas Ag/TiO_2, las mismas tienen posibilidades de poder aplicarse como catalizadores en el tratamiento de aguas contaminadas, y en dosimetría de radiaciones.

Ag/TiO_2, Fotocatálisis, Fotoluminiscencia

Citation: TIRADO-GUERRA, Salvador & VALENZUELA-ZAPATA, Miguel. Characterization of the catalytic activity and of luminescence in Ag/TiO_2 films. ECORFAN Journal-Democratic Republic of Congo 2018, 4-7: 16-26

* Correspondence to Author (email: tirado@esfm.ipn.mx)
† Researcher contributing first author.

Article **ECORFAN Journal-Democratic Republic of Congo**
December 2018 Vol.4 No.7 16-26

Introduction

Among the metal oxides that may be employed to solve problems such as environmental pollution, both in air and in water, are TiO_2, ZnO and SnO_2, among others. But is the TiO_2 the most contested for its properties such as photosensitivity, is non-toxic, economical, inexpensive (Liu, H., et al, 2013, Malagutti, A.R., et al., 2009). Given their electronic, optical, photocatalytic, and as film or powder, present various phases such as anatase (orthorhombic or tetragonal) or rutile (tetragonal), to mention the most common and of interest. Both are semiconducting broad band, with values between 3.1 to 3.3 eV (Chae, Y.K., et al, (2013), Castrejón-Sánchez, V.H., et al, (2014)); but is the anatase the most widely applied as photocatalyst by its various properties (Cruz-González, N., et al, (2013), Ochoa, Y., et al., (2010), Nada, A., et al., (2014), Yu, J., et al., (2000)). The band gap of the anatase phase allows photons interact with both the visible and UV electromagnetic spectrum. When irradiated with UV, the film of TiO_2 anatase is a source of pairs of e^- and h^+ charges, that when migrate to the surface, can interact with species of oxygen or hydroxyl ions (OH^-), the latter being produced by ionization of H_2O in the aqueous solution (Yu J. et al., 2000) or by irradiation (Malagutti, A.R., et al., (2009), Yu, J., et al., (2000)) and thus participate in redox reactions that may degrade contaminating molecules found in the environment (Chae, Y.K., et al., (2013), Yu, J., et al., (2000), Malagutti, A.R., et al., (2009)). The properties of TiO_2 films grown on substrates soda-lime exhibit good adhesion and nanostructures are fixed, as produced either by chemical spraying, by sol-gel route, precursor physical technique methods, or laser ablation, between others (Maldonado, A., et al., (2010), Tirado-Guerra, S., (2010), Yu, J., et al., (2000), Malagutti, A.R., et al., (2009), Jongnavakit P., et al., (2012), Pérez-Álvarez J., et al., (2007)).

The semiconductor films TiO_2 were prepared using the sol-gel chemistry and repeated immersion route, using precursors in solution of metal alkoxides, in equipment and technique implemented in the laboratory, controlling specific area, structure and morphology, temperature and air as well as the composition of the precursors used.

The catalytic activity of TiO_2 catalyst by itself is limited, and to improve it, it can be contaminated with precious metals or transition elements, or also complexing with other semiconductors (Liu, H., et al., (2013), Yu, J., et al., (2000)), or well a surface modification with Cu, Ti, Pd and Ag, which modifies the band gap Eg of film TiO_2, and promotes the formation of oxygen vacancies V_0 (Chae, Y.K., et al., (2013), Liu, H., et al., (2013), Yu, J., et al., (2000); Malagutti, A.R., et al., (2009)).

A semiconductor such as TiO_2 or similar systems can be excited with UV radiation and from the absorbed photons, charge carriers are generated as e^- and h^+, where the electron is ejected from the valence band (VB) leaving a hole, and transferred to the conduction band (CB), generating electron-hole pairs (Nejand, B.A., et al., (2010)). The pairs produced can participate in reactions that decompose contaminating molecules found in the environment. Catalytic semiconductor response to UV irradiation, depends on various factors: the catalyst structure, radiation, the preparation method, etc. (Xin, B., et al., (2008), Nejand, B.A., et al., (2010), Malagutti, A.R., et al., (2009), Jongnavakit P., et al., (2012)).

In this work, semiconductor Ag/TiO_2 films are synthesized and are characterized in their structure, morphology, chemical composition (EDS), topography, its optical properties, its potential photocatalytic in degradation of methyl orange (MO) under UV radiation, as well as properties of photoluminescence and emission under UV excitation, of a set of semiconductor films Ag/TiO_2 prepared by sol-gel.

The work is presented in the order: introduction-justification, experimental method, synthesis and preparation of films, film growth, characterization techniques, results, XRD, SEM and EDS, AFM, UV-Vis, X-rays photoelectron spectroscopy (XPS), photocatalysis and photoluminescence, discussion, conclusions, acknowledgments and references.

ISSN-On line: 2414-4924

Methodology experimental

Synthesis and films preparation

Oxy-acetylacetonate titanium (IV) (($C_5H_7O_2$)TiO) (Aldrich) was dissolved in 2-methoxyethanol (Aldrich, 99.3+ reagent grade) ($CH_3OCH_2CH_2OH$) (Aldrich) and monoethanolamine ($CH_2CH_2OH)NH_2$ (Aldrich) (MEA), the salt of titanium (IV) was dissolved at a 0.2 M concentration, then it was slowly added the MEA to stabilize and prevent precipitation of titanium, the solution was left under constant stirring for about 2 h at room temperature. In the preparation process, the solution was stirred until obtain a complete dissolution of the salt and achieve, a transparent solution without precipitates.

After the preparation a pH of 7 was measured and then allowed to age in a dark and cool room and from this, TiO_2 films were grown up to five layers. From a solution of silver nitrate ($AgNO_3$) films of titanium were surface modified, using the silver salt dissolved in ethanol (CH_3CH_2OH) at a low concentration, such solution was stirring for 2 h until to obtain a pH 5; the series of TiO_2 films was modified with the method already described, to obtain the Ag/TiO_2 series.

Film growth

From the prepared sol, the TiO_2 films were grown on substrates of soda-lime glass, introducing and removing the substrate from the sol repeated times, with a thickness of the films, proportional to the repetition of the process performed at room temperature. At each step the solvent and moisture were evaporated, while takes place the formation and growth of the film on the substrate in an oven at 250 °C in an air atmosphere. Finally, a heat treatment is given at 400 °C for one hour and evaporating solvents and moisture from to the film involved, while stabilizes and improves its properties. Films were grown in an oven with air, at five dives and at fixed velocity. Similarly, films of Ag/TiO_2 series were obtained with the procedure outlined, by modifying the respective surfaces with several layers of the Ag solution.

Characterization

XRD patterns of Ag/TiO_2 films were recorded with θ-2θ symmetric geometry and grade beam sample position at 0.5˚ in a PANalytical diffractometer X'pert PRO using the Kα line of Cu (λ = 0.15406 nm) with line focus, at 45 kV and 40 mA. Spectra were recorded from 3 to 60˚ with 0.05˚ step and accumulation time 150 s, but only spectra 20 to 60 degrees are presented. The Raman spectra were recorded on a LabRam spectrometer, model HR 800 and Horiba Jobin Yvon brand (400-4000 cm^{-1}).

SEM micrographs were recorded on a QUANTA 3D FEG SEM microscope (FEI) and EDS (EBSD detector EDAX). Topography was recorded by atomic force microscopy (AFM) on microscope PARK AutoProbe Equipment (Veeco) with a tip of 10 microns of silicon intermittently. The optical properties of thin films were recorded by a UV-Vis spectrophotometer Perkin Elmer, Lambda 2 UV-Vis double beam in 200-900 nm range and the glass substrate as a reference. Test photo-degradation of an aqueous solution of methyl orange (MO), was conducted to determine the absorbance of the solution when irradiated with UV-Vis light, using a reactor equipped with eight fluorescent blue lamps G8T5, 8 watts, once the film-solution, is irradiated for 10 min in a spectrometer GBC Cintra 20 model in absorbance mode and in the range of 190-600 nm. The main absorption band at 464 nm was screened during the irradiation process. Ionization states of the components O, Ti and Ag of films, were determined by X-ray photoelectron spectroscopy (XPS) in a Thermo Scientific K Alfa, dual source Mg and Al, equipment. The photoluminescence properties of Ag/TiO_2 films were recorded at room temperature in a RF-5301 Spectrofluorophotometer Shimadzu mark.

Results

X-ray diffraction

X-rays of Ag/TiO_2 films (Ag/TiO_2-p,1,4,5) (Graphic 1) were poly-crystalline (except Ag/TiO_2-5) with peaks at 25,335˚, 37,780˚, 38,565˚ and 48,022˚, associated with the planes (1 0 1), (0 0 4), (1 1 2), (2 0 0), respectively (coding 00-021-1272) and correspond to the anatase TiO_2 phase of tetragonal space group 141/amd, density 3,89 g/cm^3.

ISSN-On line: 2414-4924

Diffraction peaks were also recorded at 31,508˚, 42,821˚ and 51,354˚, with Miller indices (1 1 0), (1 0 1) and (2 1 0) of rutile phase (coding 00-021-1276) tetragonal, space group P42/mnm, with density 4,23 g/cm^3.

The anatase phase of TiO_2 was the majority one and no silver was recorded. From Scherrer's formula, $D = 0.9\lambda/\beta cos\theta$ (meaning of known parameters), the crystallite size D in the 18-24 nm range of the samples was estimated.

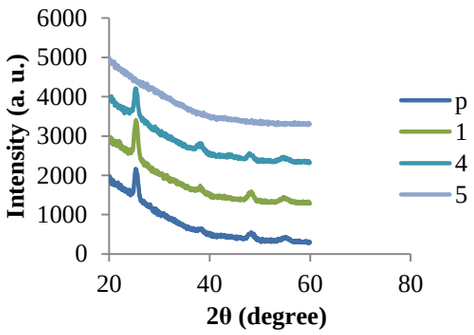

Graphic 1 XRD spectra for Ag/TiO_2 films, (p) pure, (1) one layer of Ag, (4) four and (5) five layers of Ag samples

Raman spectroscopy

The Raman spectra of Ag/TiO_2 samples prepared at 250 °C and 400 °C of treatment, were recorded in equipment already indicated. The Graphic 2a arrangement with Raman spectra of the pure sample (Ag/TiO_2-p) is shown: they are four different points and whose data are, among others: 143.206 (Eg), 198.373 (Eg), 396.655 (B1g), 516.546 (A1g) and 639,512 (Eg), vibrational modes in cm^{-1}, the data are typical modes of the anatase phase of TiO_2 systems.

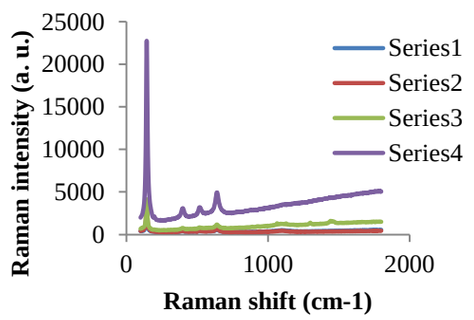

Graphic 2 Raman spectra of the pure sample TiO_2, in four different points

The Raman spectra for samples with four Ag catalyst layers (Ag/TiO_2-4) at four different points are given in Graphic 2b, the data among others: 143.206 (Eg), 256.468, 397.05 (B1g), 518.368 (A1g) and 638.547 (Eg), all in cm^{-1}, resulted; modes assigned in the literature to the anatase phase of TiO_2 (Cruz-González, N., et al., (2013)). It is observed the presence of broad bands around 1500 cm^{-1}, which do not appear in the spectra of the pure sample (Graphic 2).

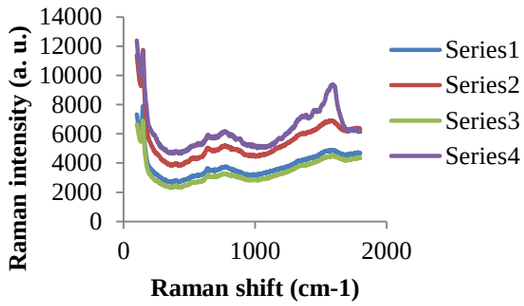

Graphic 3 Raman spectra of the sample with four Ag layers, Ag/TiO_2, at four different points

Scanning electron microscopy

SEM micrographs of Ag/TiO_2 films representative x20000 magnification are shown in Figures 1(a) and 1(b). The micrograph of the Ag/TiO_2 pure films (Figure 1a) has an uneven and porous morphology, however for micrograph in Figure 1b of the Ag/TiO_2 films with a surface deposited with Ag can be observed a morphology more uniform with fine grains and growth in areas (lights) corresponding to nanoparticles of Ag, with EDS analysis the presence of silver nanoparticles was detected, the surface distribution of the growth of the nanoparticles was uniform, making more evident the surface distribution and increased grain size (image not shown).

ISSN-On line: 2414-4924

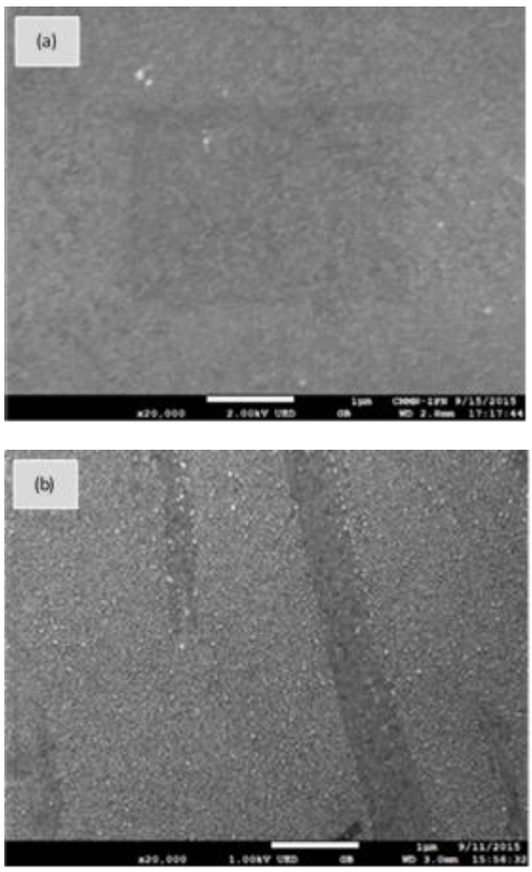

Figure 1 (a) and (b) SEM micrographs increased x20000, (a) Ag/TiO_2 pure and (b) Ag/TiO_2 samples with one layer of silver

Atomic force microscopy

From topographical images shown in the figures (Figures 2a and 2b) and (Figures 3a and 3b) of the samples, pure and that with one layer of Ag, roughness parameters Rq, Ra and Rmax were evaluated, among others, for the samples Ag/TiO_2, which are shown for three samples in Table 1. The parameters are higher in the pure sample compared to that of samples with one and four layers of Ag. The density in grains/μm^2, 3.80 and 6.32, resulted, respectively.

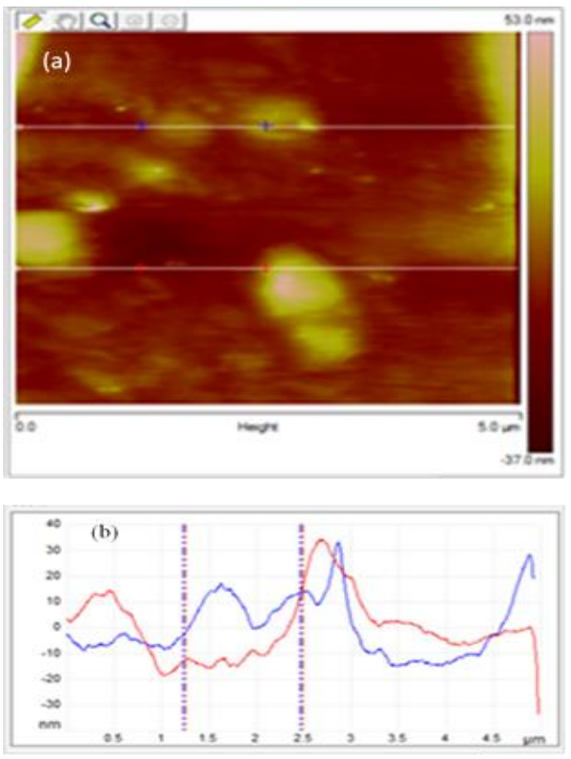

Figure 2 (a) AFM topography of Ag/TiO_2 pure sample, and (b) marked profiles

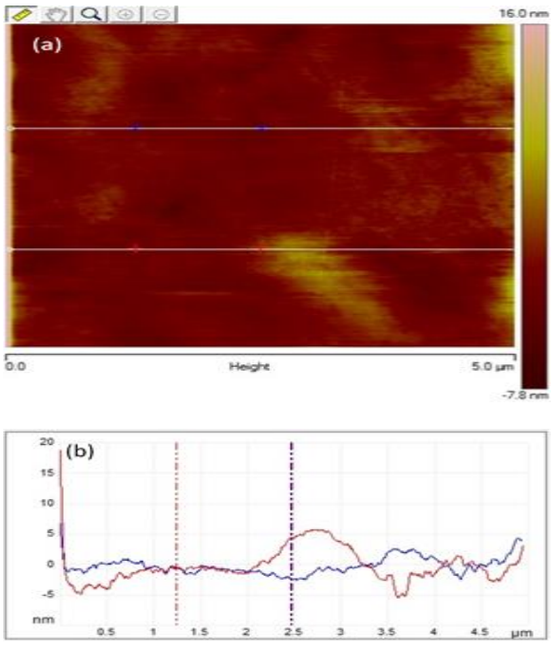

Figure 3 (a) AFM topography of Ag/TiO_2 sample with one Ag layer, and (b) marked profiles

Samples	Rms (nm)	Ra (nm)	Rmax (nm)	Av. grain (nm)	Density (g/µm2)
Ag/TiO2-p	6.03	8.5	26.2	82	3.812
Ag/TiO2-1	1.69	0.83	4.21	47	6.32
Ag/TiO2-4	1.226	0.626	18.776	22.5	9.849

Table 1 Roughness parameters for samples Ag/TiO_2, pure, one and four layers of Ag

UV-Vis microscopy

The optical properties of Ag/TiO_2 films were recorded by UV-Vis in the 190-900 nm range, using glass substrate as a reference; spectra of the sample without deposits Ag (pure) were highly transparent (Graphic 4), with increased transmittance to 90% in the visible range (400-700 nm), and the absorption board at 382 nm; from the interference effects, the thickness of pure and for samples with Ag layers, between 87-65 nm, respectively, were estimated. The transmittance of Ag/TiO_2 films decreased with the increasing of the silver layers and the absorption edge has a slight redshift. The refractive index of pure film turned between 1.149-1.550 and 1.902-2.723 for the sample with one Ag layer, in the visible range. The wide band gap Eg was evaluated for the anatase phase of TiO_2, an indirect band, from the graph $(\alpha h\nu)^{1/2}=A(h\nu-Eg)$ (Jongnaavakit, P., et al., (2012)). The values for the films were between 3.67-3.62 eV, decreasing with the Ag layers, and thus the possible improvement in film optical properties.

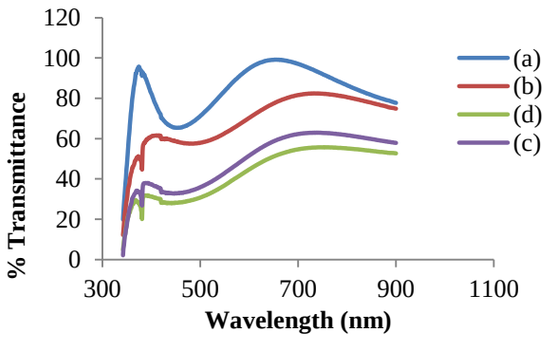

Graphic 4 UV-Vis spectra for Ag/TiO_2 films, (a) pure, (b) one layer, and (c) four and (d) layers of Ag samples

Photoelectron spectroscopy

Using photoelectron spectroscopy (XPS), the orbitals of, O1s, Ti2p, Ag3d, and ionization states of O, Ti and Ag, as well as the binding energies of the respective orbitals were evaluated; in the high-resolution spectrum of Ti2p, the spin-orbital values of 458.38 and 464.48 eV, ($2p_{3/2}$, $2p_{1/2}$), respectively, quite symmetrical, with ΔE = 5.9 eV, and also the broad band with a value of 472.48 eV, were recorded (Graphic 5). For the orbital O1s the data 529.78, 531.96 and 532.18 eV and also the higher energy value of 535.48 eV were recorded (Graphic 5). For the orbital Ag3d of the metallic state of Ag, the values were, 367.48 and 373.58 eV ($3d_{5/2}$, $3d_{3/2}$) respectively (Graphic 7).

The above data for Ti2p, O1s and Ag3d correspond to the Ag/TiO_2 systems. The energy values of the orbitals of the components of the Ag/TiO_2 films are referred to the energy of carbon C1s (284.48 eV).

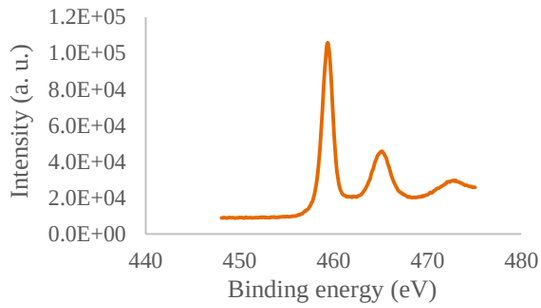

Graphic 5 High resolution XPS spectra of Ag/TiO_2 films, for Ti2p with double 458.38 and 464.48 eV, besides the signal at 472.48 eV

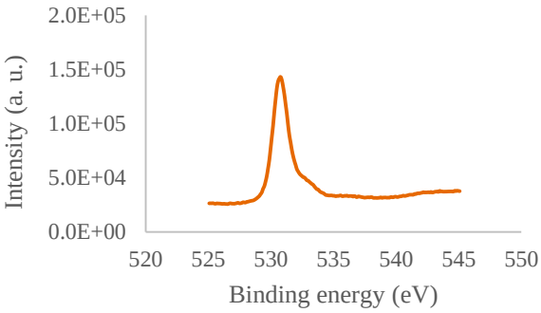

Graphic 6 High resolution XPS spectrum of Ag/TiO_2 films, for species O1s, at 529.78, 531.96, 532.18 and in 535.48 eV

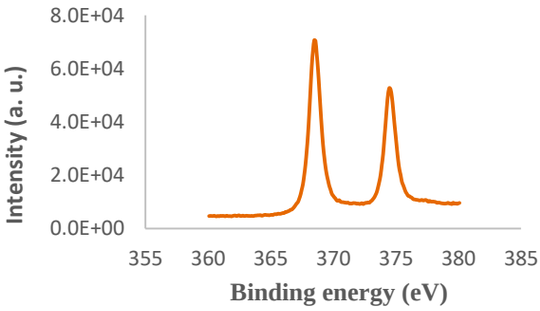

Graphic 7 For the orbital Ag3d of the metallic state of Ag, the values were, 367.48 and 373.58 eV ($3d_{5/2}$, $3d_{3/2}$) respectively

Catalytic activity

Spectra MO degradation to first cycle to 14 ppm registered for Ag/TiO_2, of pure sample, and those with one layer of Ag catalyst, are given in Graphics 7 and 8 (for the four layers arrangement of Ag, is not shown).

ISSN-On line: 2414-4924

The absorption spectrum of the aqueous solution of MO and their intensity were recorded; the intensity of the band at 464 nm is proportional to the initial concentration C_0, was monitored.

Subsequently, the film-aqueous solution, (film with area 1 cm^2, both sides), the system was irradiated each 10 min with UV light in a rectangular reactor and the absorbance of the solution is recorded, thus obtaining the concentration C of MO corresponding to time t; the process is repeated until 120 min.

The ratio of the concentration C of MO at time t, with the starting C_0 concentration, can be modeled with a kinetic equation of first order, $C = C_0\, e\text{-}kt$, where k is the pseudo constant of reaction, C is the concentration for time t, the irradiation time of the system. From Graphic 9 and the respective slopes of the systems, the better catalytic performance corresponds to that with one deposit of Ag catalyst, relative to Ag/TiO_2 pure system; Ag/TiO_2 system with four Ag layers catalyst, was the lowest performance among the three systems presented.

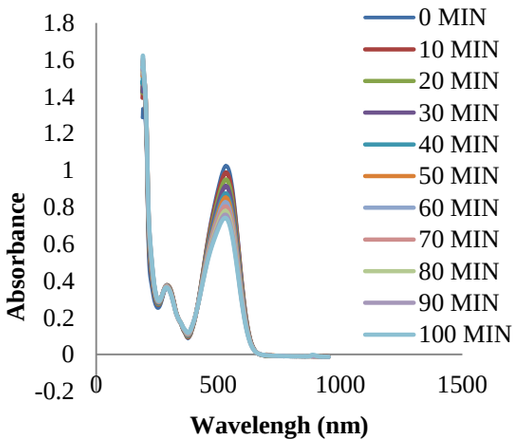

Graphic 8 Degradation process of MO by the Ag/TiO_2 pure film as a function of irradiation time

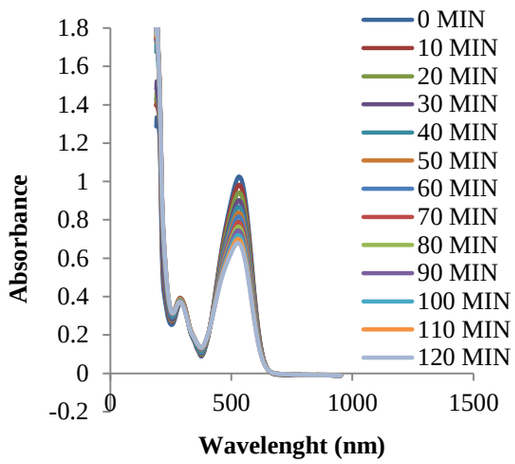

Graphic 9 Degradation process of MO by the Ag/TiO_2 film with one Ag layer, depending on the irradiation time

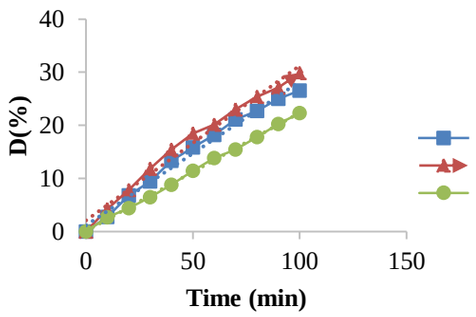

Graphic 10 Charts of the catalytic activity of Ag/TiO_2 samples corresponding to pure (p), for one (1) and four Ag layers (4)

Photoluminescence properties

The photoluminescence spectra (PL) of the Ag/TiO_2 films were recorded at room temperature in the 310 to 620 nm range with excitation energy corresponding to 325 nm. The emission spectrum of the pure sample, for the UV region in 375 nm (3.31 eV), in the intermediate region at 425 nm (2.9 eV), a wide and complex band, while in the visible region a band at 473 nm (2.62 eV) of low intensity, and the intense band at 509 nm (2.436 eV) were resolved. From the 520 nm the spectra are fading at 600 nm. The arrangement of PL spectra of three samples is given in Graph 11. By fixing the position of the main peak at 509 nm, the intensities of the Ag/TiO_2 samples are: 933.992, 899.691 and 883.056 (a.u.) of the pure, for one and four Ag deposits samples, respectively.

ISSN-On line: 2414-4924

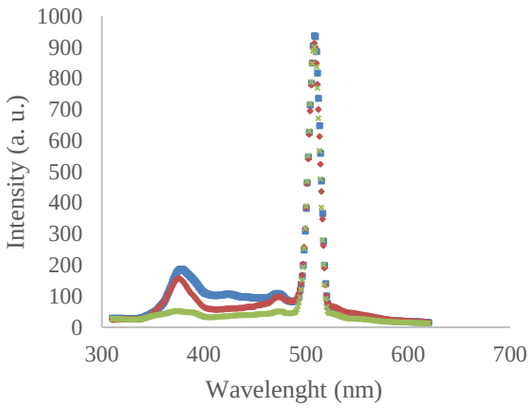

Graphic 11 Arrangement of PL spectra of Ag/TiO_2 films, for pure, one, and four Ag layers with a broadband emission at 375 nm, another around 425 nm, and the band at 473 nm, and the principal one in 509 nm

Discussion

XRD patterns of Ag/TiO_2 films were polycrystalline with the TiO_2 anatase phase and density of 3.89 g/cm^3, where also peaks of tetragonal rutile as minority phase and density of 4.23 g/cm^3 were detected. The estimated grain size for the anatase phase was between 18 to 24 nm. No silver was detected by X-rays, given the low concentration used. Grain density was higher in films with layers of silver, smaller pore size, less roughness; in general the roughness parameters evaluated in the series Ag/TiO_2 films, could explain both the optical properties and also the photocatalytic and photoluminescence ones. The Ag catalyst at low concentration incorporated superficial in the films should play an important role in such properties. The pure films were highly transparent (>90%) and also thin, and films with silver layers resulted more opaque than pure ones, such that the Eg values were affected, which could improve the catalytic activity. The band width of the Ag/TiO_2 systems were lower than those found in systems composed as ZnO/TiO_2 (Liu G., et al., (2009)).

The transmittance is greater in the pure film than those with deposits of Ag catalyst. For films Ag/TiO_2 more opaque, less light penetrates and thus become less active.

From the study by XPS, to the right of the orbital O1s intense peak, one has values: 529.78, 531.96 and 532.18 eV, and another with more energy at 535.48 eV. Within the experimental resolution, the first two values, which when adjusted, could be associated with the species O^{2-} on the network that is linked to the titanium dioxide or to the Ti-O bond, while the peak at 532.18 eV, to surface hydroxyl groups, i.e., Ti-OH or also links like C-O and C =O, because the signals overlap, the H_2O molecules are associated with the energy 535.48 eV (Malagutti, A.R., et al., (2009), Fusi, M., et al., (2011), Liu, H., et al., (2013)). The orbital Ti2p at 458.38 eV ($2p_{3/2}$) is associated with Ti^{4+} in the formula TiO_2 anatase, and the peak at 472.48 eV could be associated with a state of hybridization between orbital O2p and Ti3d; peaks at 367.48 and 373.58 eV of Ag3d correspond to the metallic state of Ag.

From Graphics 7, 8 and 9, the results of the catalytic activity of the films of pure TiO_2 systems, and those with one Ag layer in the photodegradation of MO and with four layers Ag, are shown (included in Graphic 9). The catalytic activity of the sample with one layer of Ag was better than the pure one and the sample with lowest activity corresponded to four layers of Ag, also shown; activity of pure sample is due to own surface defects because the synthesis and of the sample with one layer of Ag, that is, less transparent and less roughness than pure sample, but the silver grain size in the growth, it is felt its effect on the catalytic activity, which does not happen with the film with four layers of Ag, which is more opaque and less catalytically active.

ISSN-On line: 2414-4924

The growth procedure was similar for all systems and if something is changed, only was the number of insertions in the process and therefore a different thickness and thus a longer exposure to the drying and to treatment temperature. By the technique of sol-gel and dipping the films are obtained with surface states, defects, surface area, pore, stresses and strains, which are characteristics and very active such as the oxygen species are, or hydroxyl groups and water molecule adsorbed, that can to react with MO and degrade it (Yu, J., et al., (2000), Fusi, M., et al., (2013)), among other pollutants (Tripathi, A., et al., (2014)), with all they, the phenomenon of photoluminescence of Ag/TiO_2 could be explained, also in thin TiO_2 films, among other nanostructures as TNTs (Yu, J., et al., (2000), Fusi, M., et al., (2013), Lei, Y., et al., (2001)), oxygen vacancies and other defects are used to explain the phenomenon. Intrinsic or structural defects and impurities in metal oxide thin film and the properties thereof, are those of the synthesis, the precursor methods, the atmosphere and the heat treatment temperature (El Hichou, A., et al., (2004) and refs., De-Wei, M., et al., (2003), Lin, B., et al., (2001), Yu, J., et al., (2000), Nada, A., et al., (2014)).

PL spectra are associated with oxygen vacancies and to different types of defects of Ag/TiO_2 samples.

The peak at 375 nm, can be associated with electronic transitions between the CB and VB bands of the semiconductor Ag/TiO_2 and associated to the band gap, where the excited photoelectrons are relaxed to the bottom of the conduction band by the mechanism of phonon (Tripathi, A., et al., (2014)); the broad band at 2.9 eV, close to the board absorption band (NAB) in the pure system, with a redshift of 0.41 eV regarding the value of Eg, emissions that can be given as a recombination of free excitons (Guo, Q.X., et al., (2008), El Hichou, A., et al., (2004) and refs., De-Wei, M., et al., (2003)), the intensity of the band decreases with deposits Ag catalyst and probably decreasing luminescent centers participating in this band; the band at 475 nm (2.62 eV) could be associated with centers such as Ag acceptors or other defects.

The intense emission band in the visible (509 nm) could be associated with radiative transitions between surface or shallow vacancies (Vo^-), surface defects, commonly-donors, as Ti and deep levels of V_{Ti}, O_i, O_{Ti}, acceptor levels, between levels near the lower board of the CB and acceptor defects located at 2.436 eV below the band. This green band emission at 2.436 eV in our systems, may be sensitive to thermal treatments at different temperatures, such as those used in systems ZnO reported by Lin B., et al., (Lin, B., et al., (2001), Lim J., et al., (2004)) and/or contaminated with Ag ions (Tripathi, A., et al., (2014)); however, in the systems reported here, it shows that the emission intensity is higher in the pure sample (with treatment of one h) in relation to the broadcast of films with one Ag layer (with two h) and compared with the four layers of Ag (with four h), with a longer heat treatment.

However, here there are different samples, where the time treatment of specimens, change by coalescence and crystallite size increase relatively, so that the population of shallow levels as vacancies Vo^- or other participants, also other donors and deep levels acceptors contributing to the emission of the green region, are affected by that procedure employed; the presence of Ag^+ ion must generate an acceptor state in the region of the band gap semiconductor, acceptor level related to the low concentration that was used to modify the surface samples, although unclear the effect on the emission band; on the other hand, in doped ZnO films, the Ag dopant concentration plays an important role in UV emission photoluminescence region (Tripathi, A., et al., (2014)). In nanowires of TiO_2 anatase, Lei, Y., et al., (Lei, Y., et al., (2001) and refs. in) explain the PL spectra in the band at 424 nm, by emissions of excitons self-trapped in the TiO_6 octahedron, and for the bands at 465 and 525 nm, to oxygen vacancies, i.e. emissions from traps shallow of oxygen vacancies at 0.51 eV (band 465 nm) and 0.82 eV (band at 525 nm) below the CB, which were recorded in nanowires.

Conclusions

The Ag/TiO_2 semiconductor films were grown on substrates sodo-calcic using the sol-gel process and repeated dipping. The X-ray diffraction patterns of the Ag/TiO_2 films were polycrystalline, with a majority anatase phase respect to the rutile one.

ISSN-On line: 2414-4924

The grain size was consistent with those obtained with AFM where a higher roughness is obtained in pure films than those with Ag layers, and a grain density 3.812-9.849 (grains/μm^2). The Ag/TiO_2 films show a high transmittance, T% >90 in pure film, decreasing with Ag layers. The band gap Eg (3.67-3.62 eV) decreases with increasing Ag layers.

The orbital of components of Ag/TiO_2 films were determined, where various oxygen species (orbital O1s) that identify the O^{2-} ion in the network were determined, and associated with titanium dioxide or to the Ti-O bond, and to groups of surface hydroxyls, Ti-OH, and also the presence of H_2O molecules in the surface was identified; similarly the orbital Ti2p ($2p_{3/2}$) that is associated with Ti^{4+} in formula TiO_2 anatase and also the orbital Ag3d of the metallic state of Ag. This allowed proposing possible mechanisms to explain the photocatalytic activity of Ag/TiO_2 films in the decomposition of MO. With the surface composition of the films and the presence of various acceptor defects and also experimental conditions, photoluminescence properties can be explained. The spectra of PL at room temperature showed emission bands in the UV region, intermediate zone and in the visible region, an intense and interesting band, electronic emissions between bands and the band edge close absorption, the last bands are associated with oxygen vacancies and different types of intrinsic defects of Ag/TiO_2 samples.

The results of this study, show the potential application as catalysts and detectors of radiation in the UV-Vis range. Further studies are required with these films as well, varying the thicknesses, significant heat treatments, the MO concentration or other tracers, and higher concentrations of the Ag catalyst.

Acknowledgments

SIP-IPN Research Proyects 20171063 and 20181555, SEM, EDS, X-ray and XPS to NCNM-IPN, to Gabriela Rueda, to Natzin Tirado for editing this paper and to Ing. Omar Rios Berny by recording the photodegradation and photoluminescence spectra.

References

Castrejón-Sánchez V.H., Camps E. Camacho-López M., (2014). Quantification of phase content in TiO_2 thin films by Raman spectroscopy. Superficie y Vacío 27(3), 88-92.

Chae Y.K., Won Park J., Mori S., Suzuki M., (2013). Photocatalytic effects of plasma-heated TiO_{2-x} particles under visible light irradiation. Korean J. Chem. Eng. 30(1), 62-63.

Cruz-González N., Fernández-Muñoz J.L., Zapata-Torres M., (2013). Efecto del gas utilizado en el tratamiento térmico y la impurificación con Eu en las propiedades estructurales de nanofibras de TiO_2 depositadas por electrohilado. Superficie y Vacío 29 (3), 111-116.

De-Wei M., Zhi-Zhen Y., Jing-Yun H., Bing-Hui Z., Shou-Ke W., Hue-Hao S., Zhan-Guo W., (2003). Structural and optical characterization of $Zn_{1-x}Cd_xO$ thin films deposited by dc reactive magnetron sputtering. Chin. Phys. Lett. 20 (6), 942-943.

El Hichou A., Addou M., Bougrine A., Dounia R., Ebothé J., Troyon M., Amrani M., (2004). Cathodoluminescence properties of undoped and Al-doped ZnO thin films deposited on glass substrate by spray pyrolysis. Mat. Chem. and Phys. 83, 43-47.

Fusi M., Maccallini E., Caruso T., Casari C.S., Bassi A.L., Bottani C.E., Rudolf P., Prince K.C., Agostini R.G., (2011). Surface electronic and structural properties of nanostructured titanium oxide grown by pulsed laser deposition. Surface Science 605, 333-340.

Guo Q.X., Mitsuishi Y., Tanaka T., Nishio M., Ogawa H., (2008). Microfabrication of ZnO on a PTFE templete patterned by using synchrotron. J. Korean Phys. Soc. Vol. 53, 5, 2796-2799.

Jongnavakit P., Amornpitoksuk P., Suwanboon S., Ratana T., (2012). Surface and photocatalytic properties of ZnO thin film prepared by sol-gel method. Thin Solid Films 520, 5561-5567.

Lei Y., Zhang L.D., Meng G.W., Li G.H., Zhang X.Y., Liang C.H., Chen W. and Wang S.X., (2001). Preparation and photoluminescence of highly ordered TiO_2 nanowire arrays. Am. Inst. of Phys., DOI: 10.1063/1.1350959.

Lim J., Shin K., Kim H.O., Lee C., (2004). Photoluminescence studies of ZnO thin films grown by atomic layer epitaxy. 109, 181-185.

Lin B., Fu Z., Jia Y., (2001). Green luminescent center in undoped zinc oxide films deposited on silicon substrates. Appl. Phys. Letters 79 (7), 943-945.

Liu G., Li G., Qiu X., Li L., (2009). Synthesis of ZnO/titanate nanocomposites with highly photocatalytic activity under visible light irradiation. J. of Alloys and Compounds 481, 492-497.

Liu H., Wang J., Fan X.M., Zhang F.Z., Liu H.R., Dai J., Xiang F.M., (2013). Synthesis of CuO_2/T-ZnO_w nanocompound and characterization of its photocatalytic activity and stability property under UV irradiation. Materials Science and Engineering B 178, 158-166.

Malagutti A.R., Mauráo Henrique A.J.L., Garbin J.R., Ribeiro C., (2009). Deposition of TiO_2 and Ag:TiO_2 thin films by the polymeric precursor method and their application in the photodegradation of textile dyes. Applied Catalysis B: Environmental 90, 205-212.

Maldonado A., Mallén-Hernández S.A., Tirado-Guerra S. and Olvera M. de la L., (2010). Titanium dioxide thin films deposited by the sol-gel technique starting from titanium oxy-acetyl acetonate: gas sensing and photocatalyst applications. Phys. Status Solidi C 7, No. 9, 2316-2320.

Martínez A.I., Acosta D.R., Cedillo G., (2005). Effect of SnO2 on the photocatalytical properties of TiO2 films. Thin Solid Films 490, 118- 123.

Nada A., Moustafa Y., Hamdy A.., El-Wahab S.A., Yahea D., (2014). Synthesis and photocatalytic activity of single crystal titanate-Part-1. Chem. and Mats. Res. 6 (10), 40-49.

Ochoa Y., Ortegón., Vargas M., Rodríguez-Páez J.E., (2009). Síntesis de TiO_2, fase anatasa, por el método Pechini. Rev. Lat. de Metal. y Mater. S1 (3), 931-937.

Pérez-Álvarez J., Escobar-Alarcón L., Camps E., Romero S., Fernández-Valverde S.M., Jiménez-Becerril J., (2007). Caracterización de bicapas TiO_2/SnO_2 depositadas por ablación láser para fotocatálisis. Superficie y Vacío 20 (2), 12-16.

Tirado Guerra S., (2010). Propane gas sensing properties of SnO_2 and SnO_2:Ag thin films prepared by sol-gel technique. Cambridge Journals. MRS Online Proceedings Library, Vol. 1275, 151-158.

Tripathi A., Misra K.P., Shukla R.K., (2014). UV enhancement in polycrystalline Ag-doped ZnO films deposited by de sol-gel method. Journal of Luminescence 149, 361-368.

Yu J., Zhao X., Zhao Q., (2000). Effect of surface structure on photocatalytic activity of TiO_2 thin films prepared by sol-gel method. Thin Solid Films 379, 7-14.

ISSN-On line: 2414-4924

Article **ECORFAN Journal-Democratic Republic of Congo**
December 2018 Vol.4 No.7 27-37

Optical and photocatalytic properties of TiO_2/ZnO composites

Propiedades ópticas y fotocatalíticas de los compuestos de TiO2 / ZnO

TIRADO-GUERRA, Salvador*† & VALENZUELA-ZAPATA, Miguel

Escuela Superior de Física y Matemáticas del IPN, Edificio 9, U.P. "A.L.M." San Pedro Zacatenco, C.P. 07738, CDMEX, México. Laboratorio de Catálisis y Materiales, ESIQIE del IPN, Edificio 8, U.P. "A.L.M.", San Pedro Zacatenco, C.P. 07738, CDMEX, México.

ID 1st Author: *Salvador, Tirado-Guerra/* **ORC ID:** 000-0001-9799-9963

ID 1st Coauthor: *Miguel, Valenzuela-Zapata/* **ORC ID:** 0000-0002-8430-062X

Received July 11, 2018; Accepted November 16, 2018

Abstract

TiO_2/ZnO composites were synthesized in thin film by sol-gel route and repeated immersion and grown on soda-lime substrates. The composites were studied and characterized with various experimental techniques. TiO_2 layers were grown to five layers thick and on these several layers of ZnO were grown, forming the TiO_2/ZnO composites. The morphology and chemical composition was evaluated by SEM and EDS, phases were determined by XRD and Raman, the topography was recorded by AFM, with UV-Vis spectroscopy the optical properties, and the ionic state of components of the composition were evaluated by XPS. Porous films composed of Ti, Zn and O were identified, the TiO_2/ZnO films showed a wurtzite hexagonal structure with a crystal size of 18.0 nm; untransparent films and an *Eg* around 3.00 eV resulted. Ion states and binding energies of Ti, Zn, O and C were determined. The catalytic and photoluminescent activity of the TiO_2/ZnO composites were recorded, where MO degradation and emission spectra in the UV and visible region, were obtained. From the synthesized composites and the properties obtained from the study, as catalysts, as well as radiation detectors, were obtained in the UV-Vis range.

TiO_2/ZnO, Photodegradation, Photoluminescence

Resumen

Se sintetizaron compositos TiO_2/ZnO en película delgada por ruta sol-gel e inmersión repetida y creciéndose sobre sustratos sodo-cálcicos. Los compositos se estudiaron y caracterizaron con diversas técnicas experimentales. Se crecieron camas de TiO_2 a cinco capas de espesor y sobre éstas se crecieron diversas capas de ZnO, formando los compositos TiO_2/ZnO. La morfología y composición química se evaluó por MEB y EDS, se determinaron fases por DRX y Raman, se registró la topografía por MFA, con espectroscopia UV-Vis se evaluaron propiedades ópticas y el estado iónico de componentes del composito por XPS. Películas porosas compuestas de Ti, Zn y O se identificaron, las películas TiO_2/ZnO presentaron una estructura hexagonal wurtzita con un tamaño de cristal de 18.0 nm; películas poco transparentes y un *Eg* alrededor de 3.00 eV resultaron. Estados iónicos y energías de enlace de Ti, Zn, O y C se determinaron. Se registró la actividad catalítica y fotoluminiscente de los compuestos de TiO_2/ZnO, donde se obtuvieron la degradación de MO y los espectros de emisión en la región UV y visible. De los compositos sintetizados y las propiedades obtenidas del estudio, se obtuvieron catalizadores, así como detectores de radiación, en el rango del UV-Vis.

TiO_2/ZnO, Fotodegradación, Fotoluminiscencia

Citation: TIRADO-GUERRA, Salvador & VALENZUELA-ZAPATA, Miguel. Optical and photocatalytic properties of TiO_2/ZnO composites. ECORFAN Journal-Democratic Republic of Congo 2018, 4-7: 27-37

* Correspondence to Author (email: tirado@esfm.ipn.mx)
† Researcher contributing first author.

Article **ECORFAN Journal-Democratic Republic of Congo**
December 2018 Vol.4 No.7 27-37

Introduction

The most important semiconductor oxide is titanium dioxide (TiO_2) for its multiple applications in fields of interest in the industry, in coatings, in photocatalysis, among others (Yu, J., et al., (2000), Chae, Y.K., et al., (2013), Hermann, J.M., (1995), Hermann, J.M., et al., (1999)). In photocatalysis, the phase of interest is the anatase of TiO_2, an indirect band semiconductor with bandwidth around 3.2 eV, phase related to low temperatures, low density and is preferred, to be applied in photodegradation of polluting substances in water and the environment (Yu, J., et al., (2000), Chae, Y.K., et al., (2013), Ochoa, Y., et al., (2009), Nada, A., et. al., (2010)).

The anatase TiO_2 phase, in powders or in films on suitable substrates, is obtained with nanotube structures or other types (Ochoa, Y., et al., (2009), Nada, A., et al., (2010), Luna, A.L., et al., (2016), Giannakopoulou T., et al., (2014)). On physical methods, chemical methods are preferred, which offer several advantages. We use the sol-gel chemical route and repeated immersion to grow thin films of TiO_2, where several experimental parameters are controlled to obtain high quality films and good physical and chemical properties.

The anatase phase TiO_2 films have high adhesion to substrates of soda-calcic glass and are prepared with precursors of metal alkoxides in solutions, films with large specific area, morphology and structure, allowing to putting them in contact with various interfaces, aqueous or gaseous media, with the which can be reacting and as a consequence can be applied in heterogeneous catalysis. TiO_2 with bandwidth around 3.2 eV, to apply it in a reaction, it must be irradiated, in principle with sunlight, so little response is expected due to the low proportion of UV radiation in the solar spectrum (λ <372 nm) (Luna, A.L., et al., (2016), Castrejón-Sánchez, V.H., et al., (2014)) and since the catalyst to be useful must respond to being irradiated, generating pairs of charges (e^- and h^+), transferring charges from the valence band (VB) to the conduction band (CB), which can be used in possible oxide-reduction reactions (Luna, A.L., et al., (2016), Castrejón-Sánchez, V.H., et al., (2014)).

When the bandwidth of a catalyst, TiO_2 or ZnO, is an obstacle to be applied as such, and thus be able to degrade a tracer substance, the optical properties of the semiconductor can be improved, by impurifying the package or by superficially incorporating metals such as Cu, Ag, among others, with which it is possible to modify the properties of the semiconductor (Nada, A., et al., (2010)); also, synthesizing composite systems such as CuO-TiO_2 and testing its catalytic activity when degrading gallic acid (Luna, A.L., et al., (2016)). In a recent work, Luna, A.L., et al., (2017) report TiO_2 systems where they make bimetallic modifications, that is, they incorporate Ni and Pd to TiO_2 to improve the absorption of light, which is of interest.

Chemical reactions can be induced by the absorption of UV light by a catalyst, since photoelectrons and holes are generated, there is a separation of charges, promoting the electron to the conduction band, which can migrate to the surface of the interface between TiO_2 semiconductors and ZnO, where charge carriers can be exchanged or a reaction with the environment can be made. In addition, if there is moisture or water, it can be ionized generating hydroxyl radicals (OH^-) that are very reactive and can participate in oxide-reduction reactions, where contaminating molecules can be degraded or mineralized (Chae, Y.K., et al., (2013), Hermann, J.M., et al., (1999)). O_2 molecular oxygen can also participate by trapping a photoelectron e^- to form a defect-oxygen state, whose energy falls in the forbidden band of the semiconductor, thus having a radical super-oxide (O^{2-}) that can participate in reactions and/or in charges transitions between interfaces (Chae, Y.K., et al., (2013), Yu, J., et al., (2000)).

Thus, continuing with the composites, and using TiO_2 films as a substrate grown on glass, several layers of ZnO are deposited to generate the TiO_2/ZnO composites, of interest in this study. In addition to being characterized by several techniques, both optical and photocatalytic properties are evaluated by decomposing an aqueous solution of methyl orange (MO) at 14 ppm, in addition to evaluating the photo-luminescent response of the composites, when they are irradiated with UV light.

ISSN-On line: 2414-4924

The work is presented in the order: introduction-justification, experimental method, synthesis and preparation of films, film growth, characterization techniques, results, XRD, SEM and EDS, AFM, UV-Vis, X-rays photoelectron spectroscopy (XPS), photocatalysis and photoluminescence, conclusions, acknowledgments and references.

Methodology experimental

Synthesis and films preparation

Thin TiO_2 films were prepared from a 0.2 M sol of the titanium oxy acetylacetonate precursor salt in 2-methoxyethanol and monoethanolamine, with a 1: 1 ratio of the salt to the latter. Under constant magnetic stirring for 2 h and at room temperature, a clear solution with a pH of 7 was obtained. Thin films of TiO_2 were prepared at a thickness of five dives on soda-lime glass substrates. Part of the films were surface modified with layers of zinc oxide films, prepared from a sol of zinc acetate in 0.4 M ethanol, with a pH of 6. Thus TiO_2/ZnO composites in thin films, systems that are characterized and studied. The chemical technique of sol-gel and repeated immersion, technique implemented in the laboratory, were used (Maldonado A., et al., (2010)).

Film growth

The growth of the films on previously prepared glass substrates, was carried out by repeated immersion of the substrate and at room temperature, with a process implemented and controlled by a PC. For each immersion and extraction of the substrate from the sol, drying is carried out for 10 min at a temperature of 250 °C of the oven with air. The process is repeated until the thickness required for the film is achieved. A heat treatment is given at 300 °C for 1 hour and the films stabilize and improve their properties. A Thermoline Furnace 6000 furnace was used. The TiO_2 films (87 nm) are grown and then modified with ZnO layers (133 nm) and thus the TiO_2/ZnO composites (TZi, with i = 0, 1, 3 and 5 samples) are obtained and studied.

Characterizations

The XRD diffraction patterns of the TiO_2/ZnO films were recorded with θ-2θ symmetric geometry in a Panalytical X'pert PRO diffractometer, using the *Kα* line of *Cu* (λ = 0.15406 nm).

The Raman spectra were recorded on a LabRam spectrometer, model HR 800 and Horiba Jobin Yvon brand (400-4000 cm^{-1}). The SEM micrographs and EDS of TZi thin film composites are recorded in a JSM 7800-JEOL 4527 electronic microscope. The topography of the TZi films was recorded in a PARK AutoProbe Equipment microscope (Veeco) with a 10 μm silicon tip in the intermittent mode. The optical properties and degradation in a GBC spectrometer model Cintra 20. The ionization states of the Ti, O and Zn components of the films were determined by XPS photoelectron spectroscopy (Thermo Scientific K Alfa, Double Source Mg and Al). The emission spectra of the samples were recorded in a Shimadzu RF-5301PC spectrofluorophotometer.

Results

X-ray diffraction

The X-ray diffraction (XRD) patterns of the TZi films were polycrystalline (Graph 1) for 3 and 5 layers of ZnO and peaks at: 31,684°, 34,281°, 36,290°, 49,373°, 57,213°, wide peak at 62,162° , 68,630°, 78,822° (JCPDS 036-1451 card) (wurtzite structure of ZnO). The phases of TiO_2 was not identified. The preferential peak in the spectrum at 34,286° is associated to the plane (0 0 2) and from that the crystal size *D* is estimated according to the Debye-Scherrer ratio, $D = 0.9\lambda/\beta\cos\theta$, resulting in a *D* of 18-20 nm range. The anatase (JCPDS 021-1272) and rutile phases (JCPDS 021-1276) are not defined in this case for TiO_2.

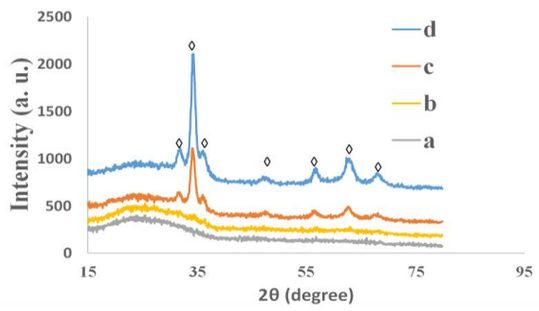

Graphic 1 Diffragrams show a) TZ0, b) TZ1, c) TZ3 and d) TZ5 samples

Raman spectroscopy

From the recorded spectra at room temperature (Graph 2) the modes: 164, 243.4, 276, 326, 356, 397, 437, 486, 514, values in cm^{-1}, were recorded. The identification of the recorded data: 326 with 340 (E2 (HL)), 356 with 380 A1 (T), 397 with 408 E1 (T), 437 with 437 (E2 (H)), values in cm^{-1}, were proposed (Ramirez Ortega D., et al., (2014)); for our ZnO films the frequencies registered in 164 and 767 cm^{-1} can be related to intermediate byproducts such as ($ZnO(OH)_2$) (López, R., et al., (2011)). Such possible assignments identify the wurtzite hexagonal phase of prepared ZnO films, as was did with XRD. Others assignments for ZnO films are given (Damen, T.C., et al., (1966), Pérez Taborda, J.A., et al., (2008)). Using Raman technique to define the phases of ZnO is required to be prepared at high temperatures and not only to the environment. On the other hand, the identification of phonons in a given system (wires, spheres, etc.) requires theoretical calculations (Lara A., del Angel, Master Thesis. (2014)).

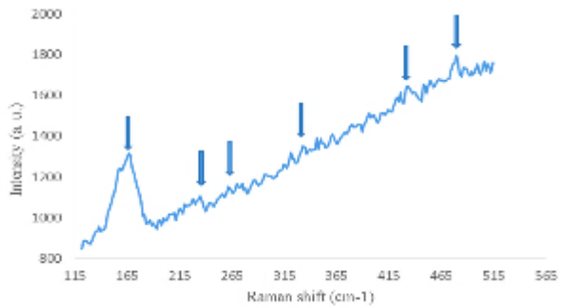

Graphic 2 Raman spectrum representative of the TZi composites

Scanning electron miscroscopy

Scanning micrographs of the TiO_2/ZnO samples, were recorded (not shown) at diffferent magnifications, especially of TZ0 and those of TZ1 with a ZnO layer, both resulted with fine grains and at higher magnification show their porosity and morphology and the presence of ZnO nanoparticles in the second case.

The analysis by EDS (Table not shown) of the TZi films, both pure and that with a deposit of ZnO, shows the presence of oxygen and titanium in the pure and also zinc in the case of sample with one ZnO layer, respectively.

Atomic force microscopy

The roughness parameters Rq, Ra and Rmax for an area 2 μm x 2 μm scanned (Table I), the parameters were of the order of nanometers, so the films are of low roughness. The micrographs (Figures 1 and 2) represent the topographic characteristics of the TZi sol-gel composites, and they show interesting surface granular formations and pores that give a contrast and a homogeneous grain size distribution in the first case (Graph 3), while a non-symmetric distribution is presented in other samples. The uniform grain size distribution in Graph 3 resulted in around 17.7 nm.

Samples	Rq (nm)	Ra (nm)	Rmax (nm)
TZ0	0.209	0.166	1.710
TZ1	0.245	0.186	2.120
TZ3	17.30	14.70	104.00

Table 1 Roughness parameters for TZ0, TZ1 and TZ3 samples

The AFM topography in Figures 1 and 2 correspond to a scale of 2 μm x 2 μm, from which the roughness parameters for the TZi samples, both TZ0 and TZ1 samples; such parameters are shown in Table 1 (TZ0, TZ1, TZ3), were evaluated. Graph 3 shows the average and uniform grain size distribution for the TZ0 sample.

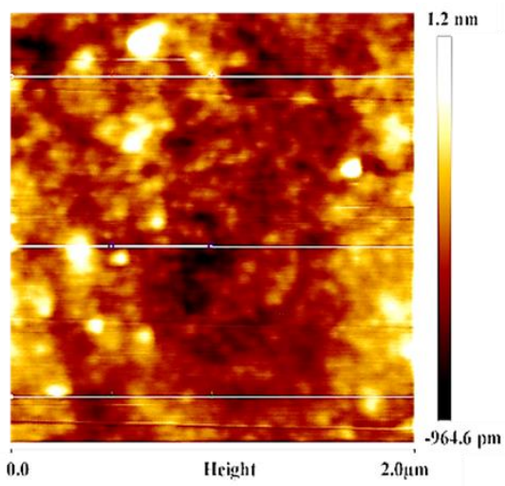

Figure 1 AFM image representative of the TZ0 sample of the series TZi under study

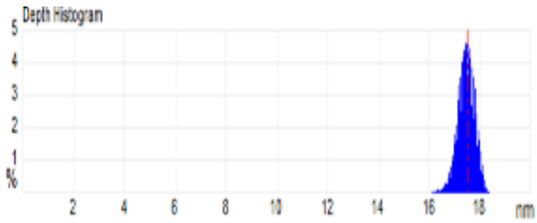

Graphic 3 Grain size distribution of the pure TZ0 sample

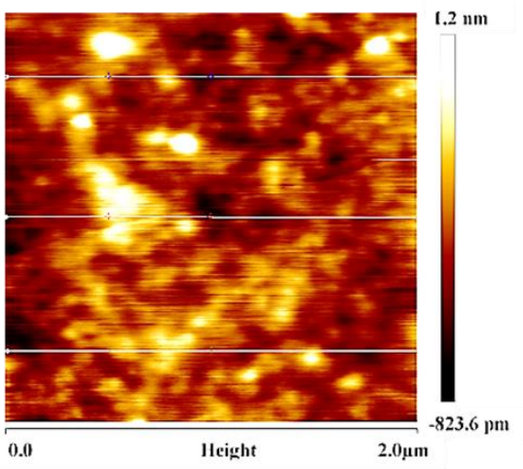

Figure 2 AFM image of film TZ1 with a ZnO layer of the series

UV-Vis spectroscopy

The spectra of the TZi samples (Graph 4) were semitransparent with absorption board at 375, 373, 343 and 399 nm, for zero, one, three and five layers of ZnO, respectively, although no congruent trend was observed; the spectra show interference effects that come from the TiO_2 growth process, although with a disorder for the first deposit of ZnO, but for three and five layers, the structural order of growth of the ZnO films appears, being clearer with five layers of ZnO. From the interference of the patterns, important parameters that characterize the films were evaluated, such as film thickness (Jongnavakit P., et al., (2012), Martínez A.I., et al., (2005)).

As the transmittance T% is recorded in the spectra and the relation of this with the reflectance (R%), the ratio $R\% = (1-T\%)/(1 + T\%)$ and that of the refractive index $n = (1 + R_{1/2})/(1-R_{1/2})$, the behavior of the index for the film is determined (Jongnavakit P., et al., (2012), Martínez A.I., et al., (2005)). The band gap *Eg* estimated, was around 3.00 eV for the pure sample and a slightly lower value is obtained for the sample with a layer of ZnO.

The Kubelka-Munk relation (Liu F., et al., (2016)) is used to estimate the band gap of the TiO_2/ZnO complex semiconductor, the graph of $(\alpha hv)^2 = A(hv - Eg)$ when extrapolated to the energy axis of the photon hv (with α zero) (Jongnavakit P., et al., (2012), Martínez A.I., et al., (2005), Pérez-Alvarez J., et al. , (2007)), with A a constant that depends on the material and α is the absorption coefficient given by the relation $\alpha(\lambda) = ln(1/T)/d$, with d the thickness of the film. There is no consistent trend in the evaluations.

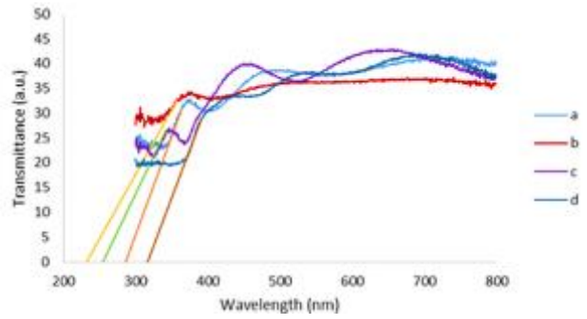

Graphic 4 UV-Vis spectra of TZi samples and slopes with Eg: TZ0 a) 2.86 eV, TZ1 b) 2.33 eV, TZ3 c) 2.55 eV and TZ5 d) 3.17 eV

XPS spectroscopy

The general spectrum of the TiO_2/ZnO composite system was recorded, which is presented in Graph 5, where the presence of the Zn2p and Ti2p orbitals, as well as oxygen and carbon, among others, are observed. The position of the bond energies of the spin-orbital Ti2p ($2p_{3/2}$ and $2p_{1/2}$) for Ti^{4+} were recorded at 458.78 eV and 464.88 eV, respectively, with a $\Delta E = 6.1$ eV (Graph 6); also it is found the 472.28 eV value, possibly associated with Ti^{3+} which gives non-stoichiometric characteristics of the surface in the films (Fusi M., et al., (2011)). The Zn2p orbitals were recorded at: 1020.98 eV ($2p_{3/2}$) and 1044.88 eV ($2p_{1/2}$) with a $\Delta E = 23.9$ eV (Graph 7). The high-resolution spectra of the O1s and of C1s orbitals were recorded, and discussed in detail below.

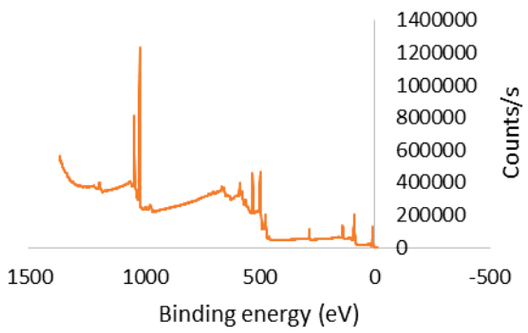

Graphic 5 General XPS spectrum showing the presence of TiO_2/ZnO composites

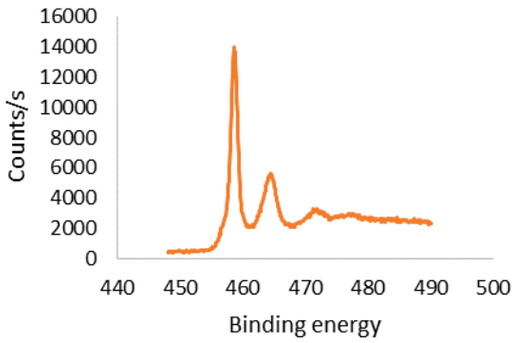

Graphic 6 Orbitals of Ti^{4+}, in 458.78 eV ($2p_{3/2}$) and in 464.88 eV ($2p_{1/2}$) with ΔE = 6.1 eV

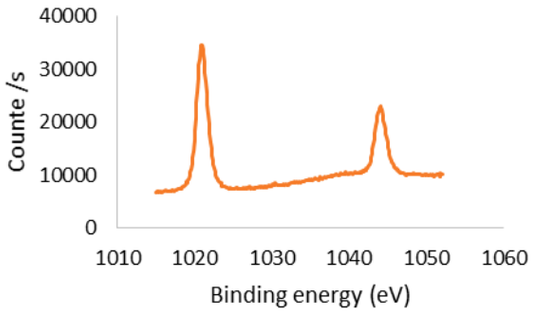

Graphic 7 Orbital Zn2p of zinc in 1020.98 eV ($2p_{3/2}$) and 1044.88 eV ($2p_{1/2}$) with ΔE = 23.9 eV

Graph 8 shows the high resolution O1s orbital spectrum of the oxygen in TiO_2/ZnO samples with the respective species according to the CasaXPS program. Measured data for the maximum were: 530.18 eV (TZ0), 529.68 eV (TZ3) and 530.18 eV (TZ5), the intensity is different in each case, and from deconvolution of spectra, were found essentially two components: the decomposition of the O1s orbital for the main component were: 530.23, 529.59 and 531. 84 eV in each case, and for the second component were: 531.03, 530.65 and 531.84 eV, respectively.

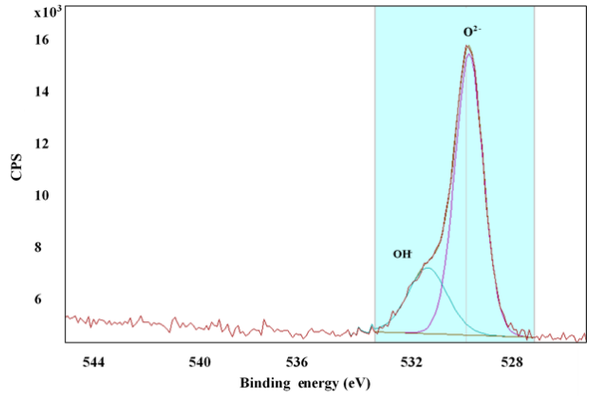

Graphic 8 Analysis of the O1s orbital for the surface oxygen of the ZnO film

The main adjustment component can be associated to O^{2-} in the network of the formula ZnO or to the bond in TiO_2 (Fusi, M., et al., (2011), Liu, F., et al., (2016) , Yu, J., et al., (2010)); the peak at 531.84 eV of the adjustment of the second component can be associated with hydroxyl OH^- and possible C-C or C = C bonds, since there are no differences detectable in energy (Liu F., et al., (2016), Fusi M ., et al. (2011), Yu J., et al., (2010)), that with temperature could be defined (Liu, F., et al., (2016); due to the registered signal and the adjustment applied, no signal was found that could be associated with H_2O molecules or other compounds such as Ti_2O_3 (Yu, J., et al., (2010)).

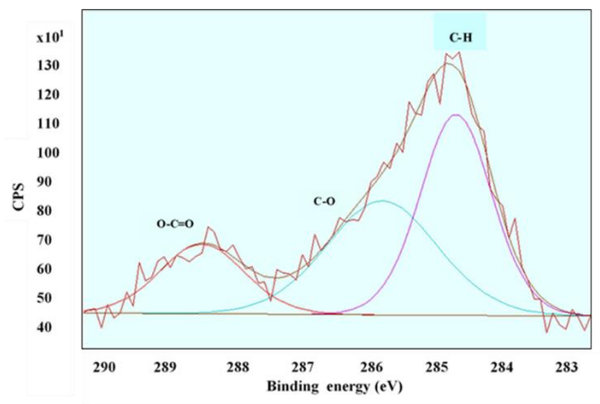

Graphic 9 Analysis of the C1s orbital for the surface carbon in the ZnO film

The type of spectrum recorded for the carbon C1s orbital is shown (Graph 9). According to the CasaXPS program and with a line shape GL(30) (Gauss-Lorentz) and records in different points from the respective sample, for the pure sample of TiO_2/ZnO (TZ0), the adjustment program yields three components or peaks with the 284.78, 286.28 and 288.08 eV values.

ISSN-On line: 2414-4924

For samples with three and five layers of ZnO, the positions change little, both in intensity and in the average width, so it can be said that there are species with different concentrations and intensities (Liu, F., et al., (2016), Yu, J., et al., (2010)). We have thus for the C1s orbital the possible groups of C-C or C-H bonds (284.78 eV), C-O (286.28 eV) and the O-C = O (288.08 eV), which would indicate different groups of organic residues on ZnO particles; the different possible signals of the adjustment come from conditions such as contact with air during the process and the heat treatment given to the samples (Liu, F., et al., (2016), Fusi, M., et al. 2011), Yu, J., et al., (2010)). All analyzed XPS spectra are referred to the C1s at 284.78 eV position of the main peak.

Catalytic activity

The photodegradation of MO at 14 ppm with TiO_2/ZnO systems was carried out in a rectangular reactor with 8 blue lamps (G8T5) with an irradiance of 7.0x200 candles/pie^2 (visible) and 2.2x200 candles/pie^2 (UVA). Graph 10 shows the degradation of MO by the pure TZ0 sample every 15 min up to 2 hours. Graph 11 shows the MO degradation of the maximum at 504 nm by the TZi samples (TZ0, TZ1, TZ3 and TZ5 samples). The response in general is low.

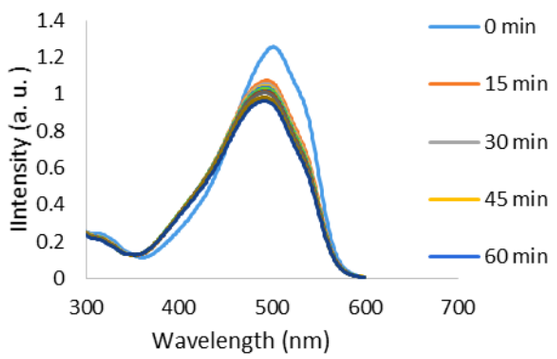

Graphic 10 First degradation cycle of MO for every 15 min up to 2 hours, of the pure TZ0 sample

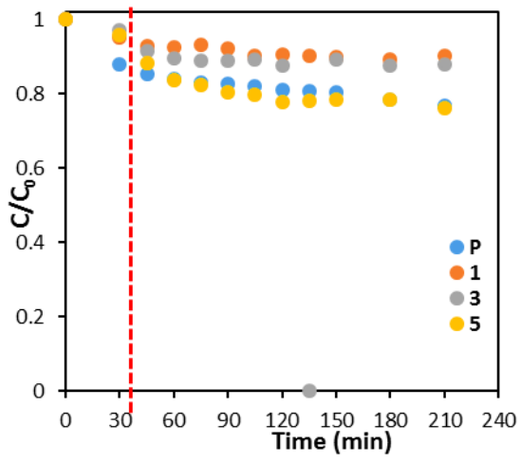

Graphic 11 Degradation of MO for every 15 min up to 2 hours, of the maximum 504 nm of each sample of the TZi series

Graphs 10 and 11 show the process of MO degradation by the TZi samples of the band around 504 nm, by irradiating the aqueous film-solution every 15 min, for a period of 2 hours.

The degradation speed of MO given by the decrease of the intensity of the indicated band, is proportional to the C concentration of the MO, according to the kinetic equation of pseudo first order, given by $C = C_0\ e^{-kt}$, with k pseudo constant of the reaction and t is the irradiation time of the study system. From the recorded data of the MO degradation process by the samples and the adjustment of the relationship between the C_0 and C concentrations for the various times t, the reaction constants of each system were evaluated, resulting in the k of the pure sample TiO_2/ZnO (TZ0) slightly higher than what is evaluated for the film TZ1 with a ZnO catalyst layer, a better response was to be expected. By increasing the catalyst should have a better response. According to Figures 1 and 2, and the roughness parameters given in Table 1, those corresponding to the composite with a ZnO layer were relatively better, however, there is no better response in the catalytic activity. In principle, roughness, surface area and grain size should play an important role in catalytic activity.

ISSN-On line: 2414-4924

The heat treatment in the film with one or more layers of ZnO, allows the grain size to grow and the number of grain boundaries to be reduced, which greatly affects the charge transfer activity between the interfaces of the composite, decreasing consequently the catalytic activity of the films; the stress states, surface defects, the quantity of hydroxyl OH^-, as well as oxygen vacancies and the specific surface area of the composite, also participate in a very important way (Yu J., et al., (2010), López R. , et al., (2011), Morales-Flores N., et al., (2011)). The optical properties recorded for the films, UV-Vis spectra, low transmittance, and interference effects and therefore a relatively low transparency, prevents the penetration of UV rays that could activate the structure of the composites.

No doubt there are more fundamental factors that explain the possible mechanisms of reactions in the film-solution interface, where the generation of hydroxyl ions (OH^-) from the humid environment or H_2O with radiation and of course the response from TiO_2/ZnO to UV radiation, where the electron-hole pairs are generated, $ZnO \rightarrow ZnO\ (e^- + h^+)$, assuming the surface of the composite, and h^+ when migrating to the semiconductor surface, or to the active sites available, will react with the OH^- ions, resulting in hydroxyl ions excited •OH, which can react and attack the MO molecule and with it the possible production of MO intermediate compounds or other less aggressive and more treatable derivatives; on the other hand, the e^- can be trapped by dissolved oxygen and produce the super oxide O^{2-}, that is, $e^- + O_2 \rightarrow O^{2-}$ (Yu J., et al., (2010)) or also the vacancies of oxygen that operate as photoelectron traps; the water molecule H_2O adsorbed turns out to be very important in the possible reactions. Therefore, the possible reactions that take place in the film-solution interface, between grain boundaries and/or charge transfer between the TiO_2/ZnO components can be explained (Yu J., et al., (2010), Lara A. del Angel (2014)).

Luminescence properties

To characterize the emission spectra (PL) of the samples in the range 300-500 nm recorded at room temperature, they were irradiated with ultraviolet light of wavelength 325 nm (3,81 eV). Thus, the emission spectra of the TiO_2/ZnO composites (TZi) shown Graph 12, were recorded.

For the TZ0 sample *a)*, the intense broadband was presented at 374,77 nm (3,308 eV) and at 389,79 nm (3,18 eV) of intensity 756,60 accounts, besides the bands in 2,82, 2,74 and 2,64 eV, the latter of greater relative intensity.

In the spectrum of TZ1 sample *b)*, a wide band with peaks in 371,69 nm (3,336 eV) and the highest peak at 381,73 nm (3,248 eV) with intensity 374,55 counts, were resolved; the peaks are resolved in 2,948, 2,863, 2,762 eV (of greater relative intensity), 2,649 eV (with structure and wide) and in 2,577 eV. For the sample TZ3 with three layers of ZnO or spectrum *c)*, there are bands in 3,246 eV (382 nm) (which are decreasing in intensity), 3,155 eV (395 nm), 2,743 eV (wide band) and that of relative intensity greater in 2,649 eV (469 nm) bands that remain. The signal in the sample TZ5 or *d)*, the band in 3,229 eV (384 nm) that decreases its intensity with respect to the previous samples, signal in 2,903 eV (that persists) (427 nm) and the broad band with structure in 2,643 eV (469 nm) that still resolves. For metal oxides such as TiO_2 or ZnO, both components of the composites, the phenomenon of photoluminescence is explained based on different types of defects, among which are the different kinds of oxygen vacancies, Ti or Zn or positions interstitial Oi, Ti, Zn, or others (Lin B., et al., (2001), Liu H., et al., (2013), Guo QX, et al., (2008), Korotcenkov G.B., et al., (2010)), which is presented in thin films of TiO_2 or other structures (Yu J., et al., (2000), Fusi M., et al., (2013), Lei Y., et al., (2001), Cruz-González N., et al., (2013)). Methods of preparing systems, precursors and heat treatment are related to structural and intrinsic defects (Lin B., et al., (2001), Yu J., et al., (2000), Nada A., et. al., (2014), Lim J., et al., (2004)).

In general, the transitions that define the photoluminescence spectra are associated to oxygen vacancies, as well as to different types of defects in the samples, which for the case of the TZ0 sample *a)*, the value of 3,308 eV would be associated with electronic transitions between the conduction band (CB) and the valence band (VB) of the TiO_2, while the 3,336 eV of TZ1 or *b)*, can be associated with the ZnO equivalent transitions of the TiO_2/ZnO system with a layer of zinc oxide; the transitions in 3,18 eV and in 3,248 eV can be associated with transitions close to the absorption edges of the respective components.

The transitions that have been identified in the spectra of the samples are generated from superficial vacancies or other types of defects (donor centers) to near or deep states at the base of the valence band (acceptor states) (Tripathi A., et. al., (2014), Lei Y., et al., (2001)). Due to the behavior of the bands in the photoluminescence spectra, which decrease in intensity or are modified, the ZnO deposit process affects the population of donor levels participating in the transitions given by phonon mechanisms or recombination of free excitons (Lin B., et al., (2001), Guo Q.X., et al., (2008), Korotcenkov G.B., et al., (2010), El Hichou A., et al., (2004) and refs. there in, De- Wei M., et al., (2003)). Oxygen vacancies and hydroxyl groups play an important role in slowing the recombination of photogenerated electron-hole pairs, which would manifest in the photocatalytic efficiency by degrading the MO of the aqueous solution (Liu G., et al., (2009), Nada A., et al., (2014), Maldonado A., et al., (2010)).

The well-defined band in the UV zone, as well as the intensity present in the emission spectra that decreases with the surface modifications of the TiO_2/ZnO composites, these systems have the possibility of being used as dosimeters in the UV region, over all the TZ0 films and those of TZ1 with a layer of ZnO. Visible transitions are maintained for both the TZ0, and the TZ1 sample corresponding to a ZnO layer (Lin B., Fu Z., Jia Y., (2001)).

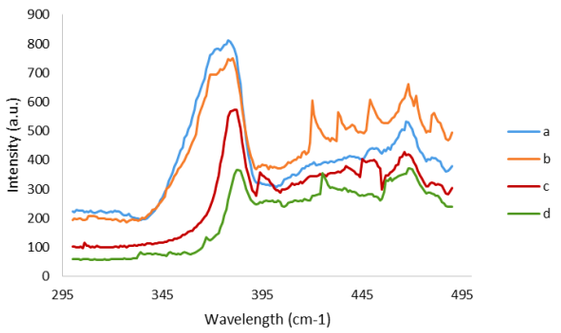

Graphic 12 Photoluminescence of the series of TZi composites, a), b), c) and d) for the four samples

Conclusions

TiO_2/ZnO (TZi) composites were synthesized in thin film with the use of sol-gel and repeated immersion. The sols were generated from titanium (IV) oxyacetylacetonate and zinc acetate, respectively. The technique was implemented in the laboratory. The film thickness at five layers of TiO_2 (TZ0) resulted around 87 nm on average, thickness that increases with the number of layers of ZnO (133 nm).

The five-layer structure of the TiO_2 substrate resulted amorphous (XRD), but the TZi composites were polycrystalline, especially those with three and five layers of ZnO. With Raman spectroscopy, the phases of anatase (TiO_2) mainly and the wurtzite phase of ZnO were confirmed separately. The morphology and composition of the composites was determined by scanning microscopy (SEM) and by electron dispersion spectroscopy (EDS) the Ti, O and Zn components of composites were identified. Porous films were recorded in the TZi composites. The topography and recorded roughness parameters (AFM) show a uniform grain distribution (17.7 nm) which is consistent with the crystal size (XRD), itself that varies with the number of ZnO layers.

By UV-Vis spectroscopy, films with low transmittance and interference effects were recorded, with absorption board around 375-399 nm. The band gap of the semiconductor *Eg* was estimated between 3.00 and 2.93 eV for the pure TiO_2 film and that with a ZnO layer, respectively.

For composites with three and five layers of ZnO the values of *Eg* are not consistent with the previous data.

The surface ionic components Ti^{4+}, Zn^{2+}, the different species of the orbital O1s (O^{2-}, hydroxyl OH^-, among others), the carbon orbital, C1s (C-C or C-H, or others), as well as their binding energies were determined by XPS. The recorded values confirm the formation of TiO_2 and ZnO, among others possible intermediate compounds, which reflect the experimental conditions.

The photodegradation of the methyl orange solution (504 nm band) (UV-Vis), by the TZi composites, irradiated with UV-Vis, resulted in the order (Graphs 10 and 11): TZ5 sample > TZ0 sample > TZ3 with three layers > TZ0 one layer of ZnO. There is no clear order that reflects the expected behaviors according to the growth conditions of the prepared films. In order to have adequate catalysts, it would be necessary to optimize them by varying experimental conditions.

ISSN-On line: 2414-4924

The emission spectra of the TZi composites (Graph 12), presented a wide emission band in the well-defined UV region and variable bands in the intermediate and visible regions. The TZ0 sample presented the UV emission of greater intensity, whereas in the TZ1 film with a layer of ZnO, the intensity decreased with respect to the first one; for three and five layers of ZnO the intensity decreases.

The emission band in the UV of the TiO_2/ZnO composites would allow these devices to be applied as dosimeters, especially the thinnest ones and photodegradation in catalysis heterogeneous.

Acknowledgments

SIP-IPN Research Proyects 20171063 and 20181555, SEM, X-ray and XPS to NCNM-IPN, to Gabriela Rueda, to Natzin Tirado for editing this paper and to Ing. Omar Rios Berny by recording the photodegradation and photoluminescence spectra.

References

Castrejón-Sánchez V.H., Camps E. Camacho-López M., (2014). Quantification of phase content in TiO_2-thin films by Raman spectroscopy. Superficie y Vacío 27(3), 88-92.

Chae Y.K., Won Park J., Mori S., Suzuki M., (2013). Photocatalytic effects of plasma-heated TiO_{2-x} particles under visible light irradiation. Korean J. Chem. Eng. 30(1), 62-63.

Cruz-González N., Fernández-Muñoz J.L., Zapata-Torres M., (2013). Efecto del gas utilizado en el tratamiento térmico y la impurificación con Eu en las propiedades estructurales de nanofibras de TiO_2 depositadas por electrohilado. Superficie y Vacío 29 (3), 111-116.

Damen T.C., Porto S.P.S., Tell B., (1966). Raman Effect in Zinc Oxide. Physical Rev. 142 (2), 570-574.

De-Wei M., Zhi-Zhen Y., Jing-Yun H., Bing-Hui Z., Shou-Ke W., Hue-Hao S., Zhan-Guo W., (2003). Structural and optical characterization of $Zn_{1-x}Cd_xO$ thin films deposited by dc reactive magnetron sputtering. Chin. Phys. Lett. 20 (6), 942-943.

El Hichou A., Addou M., Bougrine A., Dounia R., Ebothé J., Troyon M., Amrani M., (2004). Cathodoluminescence properties of undoped and Al-doped ZnO thin films deposited on glass substrate by spray pyrolysis. Mat. Chem. and Phys. 83, 43-47.

Fusi M., Maccallini E., Caruso T., Casari C.S., Bassi A.L., Bottani C.E., Rudolf P., Prince K.C., Agostini R.G., (2011). Surface electronic and structural properties of nanostructured titanium oxide grown by pulsed laser deposition. Surface Science 605, 333-340.

Guo Q.X., Mitsuishi Y., Tanaka T., Nishio M., Ogawa H., (2008). Microfabrication of ZnO on a PTFE templete patterned by using synchrotron. J. Korean Phys. Soc. Vol. 53, 5, 2796-2799.

Giannakopoulou T., Todorova N., Giannouri M., Jiaguo Yu, Trapalis C., (2014). Optical and photocatalytic properties of composite TiO_2/ZnO thin films. Catal. Today 230, 174-180.

Hermann J.M., (1995). Environmental applications of semiconductors photocatalysis. Chemical Rev. 95, 69-96.

Hermann J.M., Hoffmann M.P., Martin S.T., Choi W., Bahnemann D.W., (1999). Heterogeneous photocatalysis: fundamentals and applications to the removal of various types of aqueous pollutants. Catalysis Today 53, 115-129.

Jongnavakit P., Amornpitoksuk P., Suwanboon S., Ratana T., (2012). Surface and photocatalytic properties of ZnO thin film prepared by sol-gel method. Thin Solid Films 520, 5561-5567.

Korotcenkov G.B., Cho B.K., Nazarov M., Noh Do Y., Kolesnikova E.V., (2010). Cathodoluminiscence studies of un-doped and (Cu, Fe, and Co)-doped tin dioxide films deposited by spray pyrolysis. Current Appl. Phys. 10, 1123-1131.

Lara del Ángel A., (2014). Espectroscopia Raman de películas de GaN y ZnO para aplicaciones fotovoltaicas. Tesis Maestría.

Lei Y., Zhang L.D., Meng G.W., Li G.H., Zhang X.Y., Liang C.H., Chen W. and Wang S.X., (2001). Preparation and photoluminescence of highly ordered TiO_2 nanowire arrays. Am. Inst. of Phys., DOI: 10.1063/1.1350959.

Lim J., Shin K., Kim H.O., Lee C., (2004). Photoluminescence studies of ZnO thin films grown by atomic layer epitaxy. 109, 181-185.

Lin B., Fu Z., Jia Y., (2001). Green luminescent center in undoped zinc oxide films deposited on silicon substrates. Appl. Phys. Letters 79 (7), 943-945.

Liu F., Yan X., Chen X., Tian L., Xia Q., (2016). Mesoporous TiO_2 nanoparticles terminated with carbonate-like groups: Amorphous/crystalline structure and visible-light photocatalytic activity. Catalysis Today 264, 243-249.

Liu G., Li G., Qiu X., Li L., (2009). Synthesis of ZnO/titanate nanocomposites with highly photocatalytic activity under visible light irradiation. J. of Alloys and Compounds 481, 492-497.

Liu H., Wang J., Fan X.M., Zhang F.Z., Liu H.R., Dai J., Xiang F.M., (2013). Synthesis of CuO_2/T-ZnO_w nanocompound and characterization of its photocatalytic activity and stability property under UV irradiation. Materials Science and Engineering B 178, 158-166.

López R., Díaz T., Rosendo E., García G., Coyopol A., Juárez H., (2011). Propiedades fotoluminiscentes de películas ZnO: A-SiOx obtenidas por la técnica CVD asistido por filamento caliente. Rev. Latin. de Met. y Materiales 31 (1), 59-63.

Luna, A.L., Valenzuela M.A., Colbeau-Justin C., Vázaquez P., Rodríguez J.L., Avendaño J.R., Alfaro S., Tirado S., Garduño A., De la Rosa J.M., (2016). Photocatalytic degradation of galic acid of CuO-TiO_2 composites under UV/Vis LEDs irradiation. Applied Catalysis A: General 521, 140-148.

Luna, A.L., Dragoe E., Wang K., Beaunier P., Kowalska E., Ohtani B., Bahena Uribe D., Valenzuela M.A., Remita H., Colbeau-Justin C., (2017). Photocatalytic Hydrogen Evolution Using Ni-Pd/TiO_2: Correlation of Light Absorption, Charge-Carrier Dynamics, and Quantum Efficiency. J. Phys. Chem. C 121 (26), 14302-14311.

Maldonado A., Mallén-Hernández S.A., Tirado-Guerra S. and Olvera M. de la L., (2010). Titanium dioxide thin films deposited by the sol-gel technique starting from titanium oxy-acetyl acetonate: gas sensing and photocatalyst applications. Phys. Status Solidi C 7, No. 9, 2316-2320.

Martínez A.I., Acosta D.R., Cedillo G., (2005). Effect of SnO2 on the photocatalytical properties of TiO2 films. Thin Solid Films 490, 118- 123.

Morales-Flores N., Pal U., Sánchez Mora E., (2011). Photocatalytic behavior of ZnOand Pt-incorporated ZnO nanoparticles in phenol degradation. Applied Catalysis A: General 394, 269-275.

Nada A., Moustafa Y., Hamdy A., El-Wahab S.A., Yahea D., (2014). Synthesis and photocatalytic activity of single crystal titanate-Part-1. Chem. And Mats. Res. 6 (10), 40-49.

Ochoa Y., Ortegón., Vargas M., Rodríguez-Páez J.E., (2009). Síntesis de TiO_2, fase anatasa, por el método Pechini. Rev. Lat. De Metal. Y Mater. S1 (3), 931-937.

Pérez-Álvarez J., Escobar-Alarcón L., Camps E., Romero S., Fernández-Valverde S.M., Jiménez-Becerril J., (2007). Caracterización de bicapas TiO_2/son_2 depositadas por ablación láser para fotocatálisis. Superficie y Vacío 20 (2), 12-16.

Ramírez-Ortega D., Meléndez A.M., Acevedo-Peña P., González I., Arroyo R., (2014). Semiconducting properties of ZnO/TiO_2 composites by electrochemical measurements and their relationship with photocatalytic activity. Electrochimica Acta 140, 541-549.

Tripathi A., Misra K.P., Shukla R.K., (2014). UV enhancement in polycrystalline Ag-doped ZnO films deposited by de sol-gel method. Journal of Luminescence 149, 361-368.

Yu J., Zhao X., Zhao Q., (2000). Effect of surface structure on photocatalytic activity of TiO_2 thin films prepared by sol-gel method. Thin Solid Films 379, 7-14.

ISSN-On line: 2414-4924

[Title in Times New Roman and Bold No. 14 in English and Spanish]

Surname (IN UPPERCASE), Name 1st Author†*, Surname (IN UPPERCASE), Name 1st Coauthor, Surname (IN UPPERCASE), Name 2nd Coauthor and Surname (IN UPPERCASE), Name 3rd Coauthor

Institutional Affiliation of Author including Dependency (No.10 Times New Roman and Italic)

International Identification of Science – Techonology an Innovation,

ID 1st author: (ORC ID - Researcher ID Thomson, arXiv Author ID - PubMed Author ID - Open ID) and CVU 1st author: (Scholar-PNPC or SNI-CONACYT) (No.10 Times New Roman)

ID 1st coauthor: (ORC ID - Researcher ID Thomson, arXiv Author ID - PubMed Author ID - Open ID) and CVU 1st coauthor: (Scholar or SNI) (No.10 Times New Roman)

ID 2nd coauthor: (ORC ID - Researcher ID Thomson, arXiv Author ID - PubMed Author ID - Open ID) and CVU 2nd coauthor: (Scholar or SNI) (No.10 Times New Roman)

ID 3rd coauthor: (ORC ID - Researcher ID Thomson, arXiv Author ID - PubMed Author ID - Open ID) and CVU 3rd coauthor: (Scholar or SNI) (No.10 Times New Roman)

(Report Submission Date: Month, Day, and Year); Accepted (Insert date of Acceptance: Use Only ECORFAN)

Abstract (In English, 150-200 words)

Objectives
Methodology
Contribution

Abstract (In Spanish, 150-200 words)

Objectives
Methodology
Contribution

Keywords (In English)

Indicate 3 keywords in Times New Roman and Bold No. 10

Keywords (In Spanish)

Indicate 3 keywords in Times New Roman and Bold No. 10

Citation: Surname (IN UPPERCASE), Name 1st Author†*, Surname (IN UPPERCASE), Name 1st Coauthor, Surname (IN UPPERCASE), Name 2nd Coauthor and Surname (IN UPPERCASE), Name 3rd Coauthor. Paper Title. ECORFAN Journal-Democratic Republic of Congo. Year 1-1: 1-11 [Times New Roman No.10]

---

* Correspondence to Author (example@example.org)
† Researcher contributing as first author.

Introduction

Text in Times New Roman No.12, single space.

General explanation of the subject and explain why it is important.

What is your added value with respect to other techniques?

Clearly focus each of its features

Clearly explain the problem to be solved and the central hypothesis.

Explanation of sections Article.

Development of headings and subheadings of the article with subsequent numbers

[Title No.12 in Times New Roman, single spaced and bold]

Products in development No.12 Times New Roman, single spaced.

Including graphs, figures and tables-Editable

In the article content any graphic, table and figure should be editable formats that can change size, type and number of letter, for the purposes of edition, these must be high quality, not pixelated and should be noticeable even reducing image scale.

[Indicating the title at the bottom with No.10 and Times New Roman Bold]

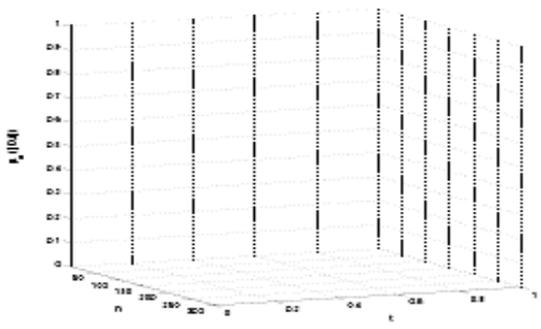

Graphic 1 Title and *Source (in italics)*

Should not be images-everything must be editable.

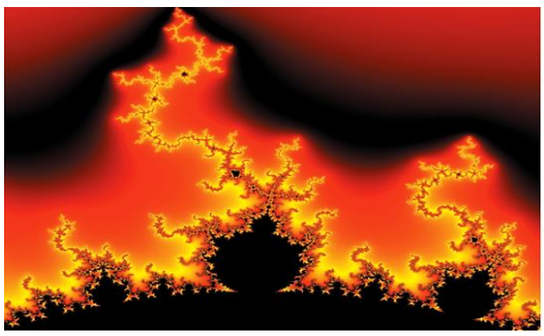

Figure 1 Title and *Source (in italics)*

Should not be images-everything must be editable.

Table 1 Title and *Source (in italics)*

Should not be images-everything must be editable.

Each article shall present separately in **3 folders**: a) Figures, b) Charts and c) Tables in .JPG format, indicating the number and sequential Bold Title.

For the use of equations, noted as follows:

$$Y_{ij} = \alpha + \sum_{h=1}^{r} \beta_h X_{hij} + u_j + e_{ij} \qquad (1)$$

Must be editable and number aligned on the right side.

Methodology

Develop give the meaning of the variables in linear writing and important is the comparison of the used criteria.

Results

The results shall be by section of the article.

Annexes

Tables and adequate sources thanks to indicate if were funded by any institution, University or company.

ISSN-On line: 2414-4924

Conclusions

Explain clearly the results and possibilities of improvement.

References

Use APA system. Should not be numbered, nor with bullets, however if necessary numbering will be because reference or mention is made somewhere in the Article.

Use Roman Alphabet, all references you have used must be in the Roman Alphabet, even if you have quoted an Article, book in any of the official languages of the United Nations (English, French, German, Chinese, Russian, Portuguese, Italian, Spanish, Arabic), you must write the reference in Roman script and not in any of the official languages.

Technical Specifications

Each article must submit your dates into a Word document (.docx):

Journal Name
Article title
Abstract
Keywords
Article sections, for example:

1. Introduction
2. Description of the method
3. Analysis from the regression demand curve
4. Results
5. Thanks
6. Conclusions
7. References

Author Name (s)
Email Correspondence to Author
References

Intellectual Property Requirements for editing:

-Authentic Signature in Color of Originality Format Author and Coauthors

-Authentic Signature in Color of the Acceptance Format of Author and Coauthors

ISSN-On line: 2414-4924

Reservation to Editorial Policy

ECORFAN-Democratic Republic of Congo reserves the right to make editorial changes required to adapt the Articles to the Editorial Policy of the Journal. Once the Article is accepted in its final version, the Journal will send the author the proofs for review. ECORFAN® will only accept the correction of errata and errors or omissions arising from the editing process of the Journal, reserving in full the copyrights and content dissemination. No deletions, substitutions or additions that alter the formation of the Article will be accepted.

Code of Ethics - Good Practices and Declaration of Solution to Editorial Conflicts

Declaration of Originality and unpublished character of the Article, of Authors, on the obtaining of data and interpretation of results, Acknowledgments, Conflict of interests, Assignment of rights and Distribution

The ECORFAN-Mexico, S.C Management claims to Authors of Articles that its content must be original, unpublished and of Scientific, Technological and Innovation content to be submitted for evaluation.

The Authors signing the Article must be the same that have contributed to its conception, realization and development, as well as obtaining the data, interpreting the results, drafting and reviewing it. The Corresponding Author of the proposed Article will request the form that follows.

Article title:

– The sending of an Article to ECORFAN-Democratic Republic of Congo emanates the commitment of the author not to submit it simultaneously to the consideration of other series publications for it must complement the Format of Originality for its Article, unless it is rejected by the Arbitration Committee, it may be withdrawn.

– None of the data presented in this article has been plagiarized or invented. The original data are clearly distinguished from those already published. And it is known of the test in PLAGSCAN if a level of plagiarism is detected Positive will not proceed to arbitrate.

– References are cited on which the information contained in the Article is based, as well as theories and data from other previously published Articles.

– The authors sign the Format of Authorization for their Article to be disseminated by means that ECORFAN-Mexico, S.C. In its Holding Democratic Republic of Congo considers pertinent for disclosure and diffusion of its Article its Rights of Work.

– Consent has been obtained from those who have contributed unpublished data obtained through verbal or written communication, and such communication and Authorship are adequately identified.

– The Author and Co-Authors who sign this work have participated in its planning, design and execution, as well as in the interpretation of the results. They also critically reviewed the paper, approved its final version and agreed with its publication.

– No signature responsible for the work has been omitted and the criteria of Scientific Authorization are satisfied.

– The results of this Article have been interpreted objectively. Any results contrary to the point of view of those who sign are exposed and discussed in the Article.

Copyright and Access

The publication of this Article supposes the transfer of the copyright to ECORFAN-Mexico, SC in its Holding Democratic Republic of Congo for its ECORFAN-Democratic Republic of Congo, which reserves the right to distribute on the Web the published version of the Article and the making available of the Article in This format supposes for its Authors the fulfilment of what is established in the Law of Science and Technology of the United Mexican States, regarding the obligation to allow access to the results of Scientific Research.

Article Title:

Name and Surnames of the Contact Author and the Coauthors	Signature
1.	
2.	
3.	
4.	

Principles of Ethics and Declaration of Solution to Editorial Conflicts

Editor Responsibilities

The Publisher undertakes to guarantee the confidentiality of the evaluation process, it may not disclose to the Arbitrators the identity of the Authors, nor may it reveal the identity of the Arbitrators at any time.

The Editor assumes the responsibility to properly inform the Author of the stage of the editorial process in which the text is sent, as well as the resolutions of Double-Blind Review.

The Editor should evaluate manuscripts and their intellectual content without distinction of race, gender, sexual orientation, religious beliefs, ethnicity, nationality, or the political philosophy of the Authors.

The Editor and his editing team of ECORFAN® Holdings will not disclose any information about Articles submitted to anyone other than the corresponding Author.

The Editor should make fair and impartial decisions and ensure a fair Double-Blind Review.

Responsibilities of the Editorial Board

The description of the peer review processes is made known by the Editorial Board in order that the Authors know what the evaluation criteria are and will always be willing to justify any controversy in the evaluation process. In case of Plagiarism Detection to the Article the Committee notifies the Authors for Violation to the Right of Scientific, Technological and Innovation Authorization.

Responsibilities of the Arbitration Committee

The Arbitrators undertake to notify about any unethical conduct by the Authors and to indicate all the information that may be reason to reject the publication of the Articles. In addition, they must undertake to keep confidential information related to the Articles they evaluate.

Any manuscript received for your arbitration must be treated as confidential, should not be displayed or discussed with other experts, except with the permission of the Editor.

The Arbitrators must be conducted objectively, any personal criticism of the Author is inappropriate.

The Arbitrators must express their points of view with clarity and with valid arguments that contribute to the Scientific, Technological and Innovation of the Author.

The Arbitrators should not evaluate manuscripts in which they have conflicts of interest and have been notified to the Editor before submitting the Article for Double-Blind Review.

Responsibilities of the Authors

Authors must guarantee that their articles are the product of their original work and that the data has been obtained ethically.

Authors must ensure that they have not been previously published or that they are not considered in another serial publication.

Authors must strictly follow the rules for the publication of Defined Articles by the Editorial Board.

The authors have requested that the text in all its forms be an unethical editorial behavior and is unacceptable, consequently, any manuscript that incurs in plagiarism is eliminated and not considered for publication.

Authors should cite publications that have been influential in the nature of the Article submitted to arbitration.

Information services

Indexation - Bases and Repositories

RESEARCH GATE (Germany)
GOOGLE SCHOLAR (Citation indices-Google)
REDIB (Ibero-American Network of Innovation and Scientific Knowledge- CSIC)
MENDELEY (Bibliographic References Manager)

Publishing Services:

Citation and Index Identification H.
Management of Originality Format and Authorization.
Testing Article with PLAGSCAN.
Article Evaluation.
Certificate of Double-Blind Review.
Article Edition.
Web layout.
Indexing and Repository
ArticleTranslation.
Article Publication.
Certificate of Article.
Service Billing.

Editorial Policy and Management

244 – 2 Itzopan Street La Florida, Ecatepec Municipality Mexico State, 55120 Zipcode, MX. Phones: +52 1 55 2024 3918, +52 1 55 6159 2296, +52 1 55 4640 1298; Email: contact@ecorfan.org www.ecorfan.org

ECORFAN®

ECORFAN Journal- Democratic Republic of Congo

2414 4924
ISSN 2414 - 4924

www.ecorfan.org